Molecular dipolar crystals as high-fidelity quantum memory for hybrid quantum computing

P. Rabl and P. Zoller
Institute for Theoretical Physics, University of Innsbruck, 6020 Innsbruck, Austria
and Institute for Quantum Optics and Quantum Information, Austrian Academy of Science, 6020 Innsbruck, Austria
(Received 20 June 2007; published 4 October 2007)

We study collective excitations of rotational and spin states of an ensemble of polar molecules, which are prepared in a dipolar crystalline phase, as a candidate for a high-fidelity quantum memory. While dipolar crystals are formed in the high-density limit of cold clouds of polar molecules under one- and two-dimensional trapping conditions, the crystalline structure protects the molecular qubits from detrimental effects of short-range collisions. We calculate the lifetime of the quantum memory by identifying the dominant decoherence mechanisms, and estimate their effects on gate operations, when a molecular ensemble qubit is transferred to a superconducting strip line cavity (circuit QED). In the case of rotational excitations coupled by dipole-dipole interactions we identify phonons as the main limitation of the lifetime of qubits. We study specific setups and conditions, where the coupling to the phonon modes is minimized. Detailed results are presented for a one-dimensional dipolar chain.

DOI: 10.1103/PhysRevA.76.042308 PACS number(s): 03.67.Lx, 33.80.Ps, 85.25.Cp, 61.50.−f

I. INTRODUCTION

In recent presentations [1,2] we have studied trapped polar molecules strongly coupled to a superconducting microwave strip line cavity, which represents a basic building block for hybrid quantum circuits, interfacing high-fidelity molecular quantum memory with solid state elements such as Cooper pair boxes (CPB) [3–6], superconducting flux qubits [7], or quantum dots [8–11]. This suggests a hybrid quantum computing scenario with the goal of combining the advantages of quantum optical and solid state implementations by interfacing molecular and solid state qubits in compatible experimental setups [12]. Polar molecules provide two key features for these interfaces. First, the long coherence times for qubits stored in polar molecules is based on identifying long-lived rotational or electron and nuclear spin states in the electronic and vibrational ground state manifold. Second, the strong coupling of molecular qubits to the microwave cavity is based on transitions between rotational excitations (in the few GHz domain), with large *electric* dipole moments of the order of a few debyes. In this context, Ref. [1] is a study of the storage of single polar molecules on electric molecular chips ~100 nm above a superconducting strip line cavity, resulting in a single molecule–single photon coupling g of up to 1 MHz. Here, the strong coupling to the microwave cavity provides the additional features of cooling of the center-of-mass motion of molecules and read out of the molecular qubits. In Ref. [2] a setup was studied (see Fig. 1), where a qubit was stored in the collective spin (or rotational) excitation of a thermal ensemble of N cold polar molecules, with the advantage of an enhanced collective coupling $g_N \equiv g\sqrt{N}$ of the qubit to the cavity (typically of the order of 1 to 10 MHz for $N=10^4-10^6$ and trapping distances ~10 μm), but at the expense of introducing dephasing of the qubit due to state-dependent collisions.

In the present work we will investigate a molecular ensemble quantum memory in the form of a *dipolar (self-assembled) crystal*. Formation of a molecular dipolar crystal (MDC) is based on inducing electric dipole moments $\mu_{\rm ind}$ of polar molecules with an external dc field, which gives a $\mu_{\rm ind}^2/4\pi\epsilon_0 r^3 \equiv C_3/r^3$ interaction between molecules at distance r. For molecules confined to one dimensional (1D) or two dimensional (2D) by an external trapping potential and dipole moments aligned perpendicular, this interaction is repulsive and allows the formation of a *high-density* crystal, where molecules perform small oscillations around their equilibrium positions, reminiscent of a Wigner crystal of trapped ions [13]. In this crystalline phase, close encounter collisions are strongly suppressed in comparison with thermal ensembles.

The paper is organized as follows. We start in Sec. II with a brief review on molecular ensemble qubits and the hybrid quantum processor proposed in Ref. [2]. In Sec. III we then study the dynamics of collective rotational excitations in a MDC due to state-dependent dipole-dipole interactions and the coupling to motional degrees of freedom. We derive a general model for this system and calculate the resulting limitations for the lifetime of ensemble qubits stored in rotational degrees of freedom. In Sec. IV we extend our model to molecules with an additional spin degree of freedom and

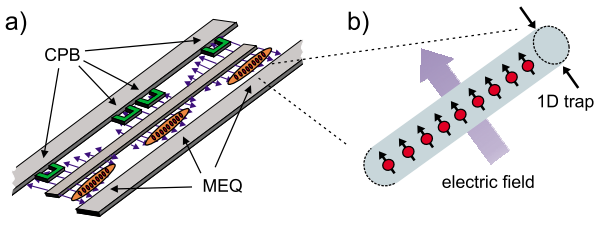

FIG. 1. (Color online) (a) Schematic picture of a hybrid quantum computer consisting of Cooper pair boxes (CPB) representing a solid state quantum processes and molecular ensemble qubits (MEQ) acting as long-lived quantum memories. Quantum information is shuttled between two systems via a superconducting strip line cavity. (b) Dipolar crystal of polar molecules. Under 1D (or 2D) trapping conditions and dipole moments aligned by a strong electric field, repulsive dipole-dipole interactions stabilize the molecules against short-range collisions. See text for more details.

show how we can realize a highly protected quantum memory using spin-ensemble qubits in a MDC. In Sec. V we discuss in some detail a potential experimental implementation of a MDC using electrostatic traps, where in particular we study the effects of an additional longitudinal confining potential. A summary and concluding remarks are given in Sec. VI.

II. OVERVIEW AND BACKGROUND MATERIAL

Before introducing our models of ensemble qubits in dipolar crystals in detail we find it useful to summarize briefly ensemble qubits and their coupling to microwave cavities, and dipolar crystals, to introduce and motivate the models for rotational and spin qubits described in the following sections.

A. Molecular ensembles coupled to a superconducting strip line cavity

We consider the setup of Fig. 1(a), where a molecular ensemble is coupled to a superconducting microwave cavity. In addition, the cavity could be coupled strongly to a CPB (or a quantum dot) representing a circuit QED system [6]. As discussed in detail in Sec. III B, molecular spectroscopy allows us to identify long-lived rotational states $|g\rangle$ and $|e\rangle$ within the electronic and vibrational ground state manifold. We assume that the ensemble of N polar molecules is prepared initially in the state $|g_1 \ldots g_N\rangle$ and is coupled to a single mode of a superconducting microwave cavity with a frequency ω_c close to the rotational transition frequency ω_{eg}. The dipole coupling between the molecules and the cavity can then be written in the form

$$H_{\text{cav-mol}} = \hbar g \sqrt{N}(R_e^\dagger c + c^\dagger R_e), \tag{1}$$

with g the single molecule vacuum Rabi frequency and c ($c^\dagger$) the cavity annihilation (creation) operator. The collective molecular operator $R_e^\dagger$ creates symmetric Dicke excitations $|n_e\rangle$ with the lowest two states

$$|0_e\rangle = |g_1 \ldots g_N\rangle,$$

$$|1_e\rangle \equiv R_e^\dagger |0_e\rangle = (1/\sqrt{N}) \sum_i |g_1 \ldots e_i \ldots g_N\rangle,$$

representing an ensemble qubit, in addition to higher excitations of the form $|2_e\rangle = (1/\sqrt{2})(R_e^\dagger)^2 |0_e\rangle$, etc. For low number of rotational excitations the operator R_e fulfills approximate bosonic commutation relations $[R_e, R_e^\dagger] \simeq 1$. As noted above, for typical experimental parameters the *collectively enhanced* coupling strength $g_N \equiv g\sqrt{N}$ can be of the order of 10 MHz, exceeding experimentally demonstrated decay rates of high-Q superconducting strip line cavities by several orders of magnitude [14,15].

For a single molecular ensemble coupled to a single CPB the total Hamiltonian for the hybrid system is

$$H_{\text{sys}} = H_{\text{CPB}} + \hbar\omega_c c^\dagger c + \hbar\omega_{eg} R_e^\dagger R_e + \hbar g_c(\sigma_+ c + \sigma_- c^\dagger) + \hbar g_N(R_e^\dagger c + c^\dagger R_e). \tag{2}$$

Here terms in the first line represent the bare Hamiltonian operators for the CPB, the cavity and the molecular ensemble. The second line of Eq. (2) contains the Jaynes-Cummings-type interaction between cavity and CPB with a vacuum Rabi frequency g_c (see Ref. [6]) as well as the molecule-cavity interaction given in Eq. (1). Interactions can in principle be controlled by tuning frequencies in and out of resonance or, as we explain later in this paper (see Sec. V D), by using a switchable Raman process. Hamiltonian (2) is readily generalized to multiple molecular ensembles and CPBs.

In summary Hamiltonian (2) provides the basic ingredient to convert the state of the CPB into a cavity photon superposition state $|\psi_c\rangle = \alpha|0_c\rangle + \beta|1_c\rangle$ [16], and in a second step to map it on an ensemble superposition

$$(\alpha|0_c\rangle + \beta|1_c\rangle)|0_e\rangle \leftrightarrow |0_c\rangle(\alpha|0_e\rangle + \beta|1_e\rangle), \tag{3}$$

and vice versa. As discussed in Ref. [2] coupling of a molecular ensemble qubit (MEQ) to higher excitations $|2_e\rangle$, etc., can be suppressed by employing the CPB as a tool to generate single photons for state preparation and as a nonlinear phase shifter to construct two qubit gates between different molecular ensembles.

For molecular ensembles to qualify as a quantum memory we not only need fast read/write operations but we also demand that the lifetime of an arbitrary ensemble superposition $|\psi_e\rangle = \alpha|0_e\rangle + \beta|1_e\rangle$ is substantially longer than coherence times of solid state qubits. The lifetime of ensemble qubits is limited by the single molecule decoherence time as well as mutual interactions. With expected single molecule decoherence rates of the order of a few Hz [1] we identify state-dependent elastic and inelastic collisions [2] between molecules as the fundamental limitation of the lifetime of a molecular ensemble quantum memory stored in a thermal gas of molecules.

B. Dipolar crystal

To avoid collisional dephasing while still keeping the benefit from a collectively enhanced coupling we consider molecular ensemble qubits prepared in a high-density crystalline phase under 1D or 2D trapping conditions. Dipolar crystals of molecules have recently been studied in Ref. [17], where it has been shown that with dipole moments aligned by an external dc electric field molecules are stabilized by repulsive dipole-dipole interactions $V_{dd} = C_3/r^3$ in a plane perpendicular to the bias field. Attractive interactions along the remaining direction are suppressed by a strong transverse confinement [17,18]. Under such conditions the low-temperature physics of the molecules is characterized by the dimensionless parameter

$$\gamma = \frac{E_{\text{pot}}}{E_{\text{kin}}} \equiv \frac{\mu_{\text{ind}}^2/(4\pi\epsilon_0 a_0^3)}{\hbar^2/m a_0^2} = \frac{C_3 m}{\hbar^2 a_0}, \tag{4}$$

which is the ratio between potential energy and kinetic energy for molecules of mass m for a given density $n = 1/(a_0)^d$ and dimension $d = 1, 2$. For $\gamma \gg 1$ the dipolar repulsion wins over kinetic energy leading to the formation of a crystalline phase, i.e., small oscillations of the molecules around their equilibrium values. The formation of a dipolar

crystal at *high* densities, i.e., in the limit where collisions are most damaging is in contrast to the familiar Wigner crystal for trapped ions or electrons where crystallization occurs at *low* densities. Numerical Monte Carlo simulations [17,19–21] have predicted a crystalline phase for $\gamma \gtrsim 1$ in 1D and $\gamma \gtrsim 20$ in 2D. For typical experimental numbers a stable crystal of polar molecules is found for a lattice spacing a_0 of a few times 100 nm.

C. Ensemble qubits in dipolar crystals

In the following sections we address the question whether it is possible to achieve a stable molecular crystal *and* at the same time encode quantum information in ensemble superpositions $|\psi_e\rangle = \alpha|0_e\rangle + \beta|1_e\rangle$. In this context we distinguish between two types of ensemble qubits: (i) rotational qubits, i.e., the states $|0_e\rangle$ and $|1_e\rangle$ introduced above, and (ii) spin qubits. In Sec. III we first consider rotational ensemble qubits which are directly affected by state-dependent dipole-dipole interactions and decay by phonon-induced scattering processes out of the symmetric state $|1_e\rangle$. In Sec. IV we extend our model to molecules with an additional spin degree of freedom and study ensemble qubits encoded in collective excitations of two spin states $|g\rangle$ and $|s\rangle$ within the same rotational manifold. As spin degrees of freedom are essentially unaffected by dipole-dipole interactions, spin-ensemble qubits in a MDC form indeed a highly protected quantum memory. However, a degrading of the spin-ensemble quantum memory due to dipole-dipole interactions still occurs during gate operations when molecules are (virtually) excited into the rotational state $|e\rangle$. To estimate the resulting gate fidelities under realistic experimental conditions we focus in Sec. V on a specific implementation of a 1D dipolar crystal and include effects of an additional longitudinal confining potential into our model.

III. ROTATIONAL ENSEMBLE QUBITS IN A HOMOGENEOUS DIPOLAR CRYSTAL

In this section we consider the properties of ensemble qubits with N molecules prepared in a crystalline phase, and qubits encoded in collective rotational excitations. Our goal is to study the dynamics, and thus decoherence, of an initial rotational ensemble qubit $|\psi_e\rangle = \alpha|0_e\rangle + \beta|1_e\rangle$ under the influence of dipole-dipole interactions. We start with the simplest possible model of a homogeneous 1D or 2D crystal, returning to questions of experimental implementations and requirements (e.g., questions of transverse and longitudinal trapping potentials, and the choice of particular molecular states) at a later stage.

A. Hamiltonian

Let us consider an *(infinite) homogeneous* dipolar crystal of a given density corresponding to a lattice spacing a_0, which is initially prepared in the qubit state $|0_e\rangle = |g_1 \ldots g_N\rangle$. We denote by $\mathbf{r}_i^0$ the classical equilibrium positions of the molecules, which form a linear chain in 1D or a triangular lattice in 2D. As discussed in Sec. II, the stability of the crystal requires $\gamma = C_3 m/\hbar^2 a_0 \gg 1$, where now $C_3 = \mu_g^2/4\pi\epsilon_0$ is determined by μ_g, the induced dipole moment of state $|g\rangle$. The dynamics of the system including internal and motional degrees of freedom is given by the Hamiltonian

$$H_{\mathrm{MDC}} = \sum_i \left(\frac{\mathbf{p}_i^2}{2m} + \hbar\omega_{eg}|e_i\rangle\langle e_i| \right) + \hat{V}_{dd}(\{\mathbf{r}_i\}), \qquad (5)$$

with 1D or 2D position and momentum operators denoted by $\mathbf{r}_i$ and $\mathbf{p}_i$, respectively, and ω_{eg} the transition frequency between states $|e\rangle$ and $|g\rangle$. The Hamiltonian (5) is the sum of the kinetic energies of the molecules, a bare molecular Hamiltonian for the internal (rotational) states, and the dipole-dipole interaction $\hat{V}_{dd}(\{\mathbf{r}_i\})$ which couples the internal and motional degrees of freedom. With $\boldsymbol{\mu}$ denoting the electric dipole operator of the molecule the dipole-dipole interaction is given by

$$\hat{V}_{dd}(\{\mathbf{r}_i\}) = \frac{1}{8\pi\epsilon_0} \sum_{i \neq j} \frac{\boldsymbol{\mu}_i \cdot \boldsymbol{\mu}_j - 3(\mathbf{n}_{ij} \cdot \boldsymbol{\mu}_i)(\mathbf{n}_{ij} \cdot \boldsymbol{\mu}_j)}{|\mathbf{r}_i - \mathbf{r}_j|^3}, \qquad (6)$$

where $\mathbf{n}_{ij} = \mathbf{r}_{ij}/|\mathbf{r}_{ij}|$ is the unit vector pointing along direction $\mathbf{r}_{ij} = \mathbf{r}_i - \mathbf{r}_j$.

To study the dynamics of ensemble states $|0_e\rangle$ and $|1_e\rangle$ under the action of H_{MDC} we proceed as follows. Since in the crystalline phase molecules are located around equilibrium positions $\mathbf{r}_i \approx \mathbf{r}_i^0$, we describe in a first step the action of the internal operator $\hat{V}_I \equiv \hat{V}_{dd}(\{\mathbf{r}_i^0\})$ on the qubit state $|1_e\rangle$. As the dipole-dipole interactions depend on the actual choice of rotational states $|g\rangle$ and $|e\rangle$ we start with a short overview on rotational spectroscopy of polar molecules in Sec. III B. In Sec. III C we then discuss the action of dipole-dipole interactions on ensemble states $|0_e\rangle$ and $|1_e\rangle$. We find that at least in a homogeneous crystal the only effect of $\hat{V}_I$ is an energy shift for state $|1_e\rangle$ which does not destroy the decoherence of a qubit state $|\psi_e\rangle$. Therefore, in Sec. III E we include molecular motion and write the position operator of each molecule as $\mathbf{r}_i = \mathbf{r}_i^0 + \mathbf{x}_i$, with $\mathbf{x}_i$ accounting for small fluctuations around the classical equilibrium positions $\mathbf{r}_i^0$. By expanding $\hat{V}_{dd}(\{\mathbf{r}_i\})$ in powers of $\mathbf{x}_i$ we obtain the dominant contributions for the interactions between internal and external degrees of freedom which, for example, account for state-dependent forces on the molecules due to a difference of the induced dipole moments of states $|g\rangle$ and $|e\rangle$. The analysis of the resulting model given in Sec. III F finally allows us to estimate the ensemble quantum memory lifetime, T_e, for a wide range of system parameters.

B. Rotational spectroscopy

Since the interactions between molecules depend on the actual choice of rotational states $|g\rangle$ and $|e\rangle$ we will first summarize the rotational spectroscopy of polar molecules in the presence of external electric fields [22]. To keep the discussion on a basic level we consider in this section only molecules like SrO or CsRb with a closed electron shell and a $^1\Sigma$ electronic ground state. In Sec. IV we extend our model to molecules with additional spin degrees of freedom.

At sub-Kelvin temperatures with electronic and vibrational degrees of freedom frozen out the energy spectrum of

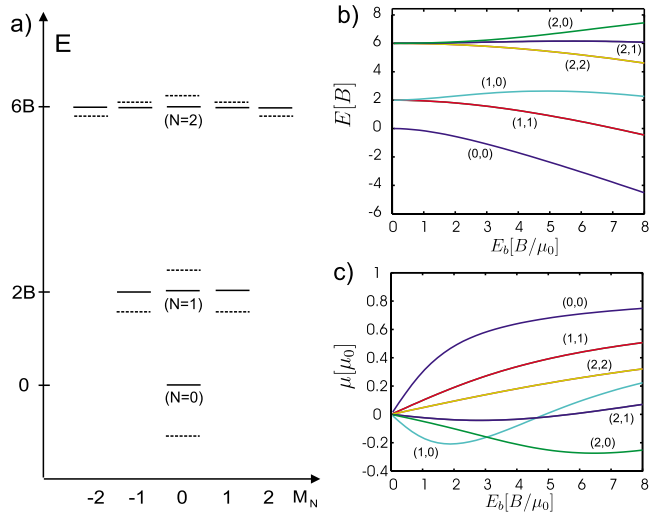

FIG. 2. (Color online) (a) Rotational energy spectrum for zero bias field $E_b=0$ (solid lines) and the corresponding shifted energy levels at $E_b=3B/\mu_0$ (dashed lines). (b) Energies spectrum and (c) induced dipole moments $\mu_i=\langle i|\mu_z|i\rangle$ for the lowest few eigenstates as a function of the applied bias field E_b. Different curves for eigenstates $|N,M_N\rangle_{E_b}$ are labeled by $(N,|M_N|)$.

a $^1\Sigma$ molecule is well described by the rigid rotor Hamiltonian $H_M=B\mathbf{N}^2$ with $\mathbf{N}$ the angular momentum of the nuclei and B the rotational constant which is typically in the order of several GHz. In the presence of an external electric bias field $\mathbf{E}_b$, polar molecules interact with the field via the dipole coupling $-\boldsymbol{\mu}\mathbf{E}_b$, with $\boldsymbol{\mu}$ the electric dipole operator of the molecule. In the following we choose our z axis along the direction of the bias field, i.e., $\mathbf{E}_b=E_b\mathbf{e}_z$ and the total Hamiltonian is $H_M=B\mathbf{N}^2-\mu_z E_b$.

For a given electric field we label eigenstates of H_M as $|N,M_N\rangle_{E_b}$ with M_N the eigenvalue of the operator N_z. In the field free case ($E_b=0$) the eigenstates $|N,M_N\rangle_0$ are the usual angular momentum eigenfunctions and the corresponding anharmonic energy spectrum, $E_N=B(N+1)N$, with energy levels $(2N+1)$-fold degenerate is shown in Fig. 2(a). In the presence of an electric bias field ($E_b\neq 0$) the dipole coupling mixes different angular momentum eigenfunctions and general eigenstates $|N,M_N\rangle_{E_b}$ are superpositions of states $|N,M_N\rangle_0$ with different N but with the same M_N quantum number. The modified rotor spectrum as a function of the applied electric field E_b is shown in Fig. 2(b). The spectrum retains its anharmonicity over a wide range of electric fields values and only for $E_b\gg B/\mu_0$ with μ_0 the axis fixed dipole moment of the molecule rotational excitations become approximately harmonic.

The mixing of different rotational states $|N,M_N\rangle_0$ in the presence of an electric field corresponds to an alignment of the molecules along the field direction, and in general an eigenstate $|\phi\rangle=|N,M_N\rangle_{E_b}$ exhibits a finite-induced dipole moment $\langle\phi|\mu_z|\phi\rangle\neq 0$ along the z direction. The magnitude and sign of the induced dipole moments depend on the specific state and the strength of the bias field E_b. The induced dipole moments for the lowest rotational states are plotted in Fig. 2(c) as a function of the electric field E_b. We find that for an axis fixed dipole moment $\mu_0\approx 5-10$ D and moderate electric fields, $E_b\approx 2B/\mu_0$, which typically corresponds to a few kV/cm, induced dipole moments of a few debyes can be achieved. Note that in general induced dipole moments of nondegenerate states are different, although there are certain values of the bias field, so-called "sweet spots" [1], where induced dipole moments for two states are the same.

The anharmonicity of the rotor spectrum for low and moderate electric fields allows us to choose two rotational states, e.g., $|g\rangle=|N,M_N\rangle_{E_b}$ and $|e\rangle=|N',M_N'\rangle_{E_b}$, which are selectively coupled by a dipole transition to the fields of a microwave cavity of appropriate frequency and polarization. Selection rules for dipole transitions require $\Delta M_N=0,\pm 1$, while the additional restriction $\Delta N=\pm 1$ applies only for vanishing E_b. In the following the states $|g\rangle$ and $|e\rangle$ form our truncated single molecule basis which defines our ensemble states $|0_e\rangle$ and $|1_e\rangle$, as introduced in Sec. I.

C. Dipole-dipole interactions

So far we have discussed ensemble qubits on the level of independent molecules. As the crystalline phase is stabilized by mutual interactions between molecules, which for different internal states depend, e.g., on the different induced dipole moments, we proceed to study dipole-dipole interactions given in Eq. (6).

Consider the action of $\hat{V}_{dd}$ on the qubit states. For fixed positions $\mathbf{r}_i$ we define the operator acting on the internal states,

$$\hat{D}_{ij}(\mathbf{n}_{ij})=\boldsymbol{\mu}_i\cdot\boldsymbol{\mu}_j-3(\mathbf{n}_{ij}\cdot\boldsymbol{\mu}_i)(\mathbf{n}_{ij}\cdot\boldsymbol{\mu}_j). \tag{7}$$

We will simplify $\hat{D}_{ij}(\mathbf{n}_{ij})$ under the assumption that its action is confined to the two molecule subspace $\mathcal{H}_{ij}=\{|\epsilon_i,\epsilon_j\rangle,\epsilon_i=g,e\}$ and that it is independent of $\mathbf{n}_{ij}$ when molecules are confined in the (x,y) plane. This simplification is possible under the following conditions. First, due to the comparatively large separation between molecules of $|\mathbf{r}_{ij}|\gtrsim 100$ nm the dipole-dipole interaction is a weak perturbation on the scale of the rotational spectrum ($\sim B$). This is true for most choices of states $|g\rangle$ and $|e\rangle$ and allows us to restrict the action of the operator $\hat{D}_{ij}(\mathbf{n}_{ij})$ to the subspace $\mathcal{H}_{ij}$. There are exceptions, e.g., the combination $|g\rangle=|N,0\rangle$ and $|e\rangle=|N',+1\rangle$ where the degeneracy between the states $|N',1\rangle$ and $|N',-1\rangle$ would lead to resonant transitions out of $\mathcal{H}_{ij}$. We can nevertheless include those combinations of states in our discussion when we assume that the degeneracy is lifted, e.g., by additional ac microwave fields. Our second assumption is that with molecular motion restricted to the (x,y) plane, i.e., $\mathbf{n}_{ij}\perp\mathbf{e}_z$ the operator $\hat{D}_{ij}(\mathbf{n}_{ij})$ is independent of $\mathbf{n}_{ij}$. This condition is fulfilled for $|g\rangle$ and $|e\rangle$ being eigenstates of N_z. For other states, e.g., $|e\rangle$ as eigenstate of the operator N_x, the directional dependence of $\hat{D}_{ij}(\mathbf{n}_{ij})$ would lead to an additional x/y dependence in the models for 2D crystals derived below. For simplicity we ignore these cases in the following discussion.

With these assumptions we decompose $\hat{D}_{ij}=\hat{D}_{ij}^{(i)}+\hat{D}_{ij}^{(r)}$. The first term, $\hat{D}_{ij}^{(i)}$, describes a state-dependent interaction

due to a difference in the induced dipole moments, $\delta\mu=\mu_e-\mu_g$, with $\mu_i=\langle i|\mu_z|i\rangle$. It is diagonal in the qubit basis and we can write it as

$$\hat{D}_{ij}^{(i)}=(\mu_g\mathbb{1}_i+\delta\mu|e_i\rangle\langle e_i|)(\mu_g\mathbb{1}_j+\delta\mu|e_j\rangle\langle e_j|). \tag{8}$$

The second term, $\hat{D}_{ij}^{(r)}$, accounts for resonant exchange of rotational quanta between molecules. Introducing a Pauli operators notation $\sigma_i^+=|e_i\rangle\langle g_i|$, etc., it is given by

$$\hat{D}_{ij}^{(r)}=D_r(\sigma_i^+\sigma_j^-+\sigma_i^-\sigma_j^+), \tag{9}$$

with the matrix element $D_r=\eta|\langle e|\boldsymbol{\mu}|g\rangle|^2$, where $\eta=1$ for rotational states of equal quantum number M_N and $\eta=-1/2$ for $M_N'=M_N\pm1$.

While the diagonal operator $\hat{D}_{ij}^{(i)}$ acting on the qubit states leads to a state-dependent energy shift, the operator $\hat{D}_{ij}^{(r)}$ flips the rotational excitations between neighboring molecules. When motional degrees of freedom are included, both processes result in state-dependent forces on the molecules.

D. Effect of dipole-dipole interactions for fixed lattice positions

Let us consider the simple situation where the molecules are frozen at lattice positions $\mathbf{r}_i^0$. In this case the dipole-dipole interaction takes on the form

$$\hat{V}_I=\frac{1}{8\pi\epsilon_0}\sum_{i\neq j}\frac{\hat{D}_{ij}}{|\mathbf{r}_i^0-\mathbf{r}_j^0|^3}. \tag{10}$$

In view of $[\hat{V}_I,R_e^\dagger]\sim R_e^\dagger$ both ensemble qubit states $|0_e\rangle$ and $|1_e\rangle$ are eigenstates of $\hat{V}_I$. Therefore, apart from a small energy shift, the internal part of the dipole-dipole interactions does not limit the lifetime of the ensemble qubit. This statement, of course, ignores inhomogeneity and finite size effects which depend on the specific experimental setup (see Sec. V). However, these imperfections can in principle be avoided and do not constitute a fundamental restriction to ensemble quantum memories in dipolar crystals. We conclude that in our model state-dependent forces and the resulting entanglement with motional degrees of freedom is the primary source of decoherence.

E. Effect of dipole-dipole interactions including motional couplings

We return to the full Hamiltonian H_{MDC} given in Eq. (5) which includes internal as well as external degrees of freedom.

1. Decomposition of the dipole-dipole interactions acting on internal and motional degrees of freedom

With the assumption that the dipole-dipole interaction is confined to the subspace $\mathcal{H}_{ij}=\{|\epsilon_i,\epsilon_j\rangle,\epsilon_i=g,e\}$, we write

$$\hat{V}_{dd}(\{\mathbf{r}_i\})=\frac{\mu_g^2}{8\pi\epsilon_0}\sum_{i\neq j}\frac{\mathbb{1}_{ij}+\hat{K}_{ij}}{|\mathbf{r}_i-\mathbf{r}_j|^3}, \tag{11}$$

where we introduced the dimensionless operator $\hat{K}_{ij}$ by

$$\hat{D}_{ij}\equiv\mu_g^2(\mathbb{1}_{ij}+\hat{K}_{ij}). \tag{12}$$

This decompositions separates $\hat{V}_{dd}$ into a part which is independent of the internal state and describes purely repulsive interaction between molecules which stabilize the crystal. All state-dependent properties of $\hat{V}_{dd}$ are contained in the operator $\hat{K}_{ij}$ given by

$$\hat{K}_{ij}=\epsilon(|e_i\rangle\langle e_i|+|e_j\rangle\langle e_j|)+\kappa(\sigma_i^+\sigma_j^-+\sigma_i^-\sigma_j^+). \tag{13}$$

Here $\epsilon=(\mu_e-\mu_g)/\mu_g$ is the normalized difference of induced dipole moments, and $\kappa=D_r/\mu_g^2$ is the normalized coupling constant for resonant exchange processes. Note that in Eq. (13) we have omitted the term $\epsilon^2|e_i,e_j\rangle\langle e_i,e_j|$ which is negligible for a low number of rotational excitations, as is the case for our initial ensemble qubit. Therefore, for a given choice of states $|g\rangle$ and $|e\rangle$ we characterize dipole-dipole interactions by the induced dipole moment of the ground state μ_g, and the two dimensionless parameters ϵ and κ.

We rewrite the molecular position operators as $\mathbf{r}_i=\mathbf{r}_i^0+\mathbf{x}_i$ and expand Eq. (11) in $\mathbf{x}_i$, so that the dipole-dipole interaction splits into three contributions,

$$\hat{V}_{dd}(\{\mathbf{r}_i\})=\hat{V}_I+\hat{V}_E(\{\mathbf{x}_i\})+\hat{V}_{\mathrm{int}}(\{\mathbf{x}_i\}), \tag{14}$$

with $\hat{V}_I$ ($\hat{V}_E$) acting on internal (external) degrees of freedom, respectively, while $\hat{V}_{\mathrm{int}}$ contains all remaining terms which couple the external and internal dynamics.

2. Excitons: Rotational excitations hopping on the lattice

Let us first return to the internal operator $\hat{V}_I$ defined in Eq. (10), where by neglecting a global energy shift we can replace operators $\hat{D}_{ij}$ by $\mu_g^2\hat{K}_{ij}$. The operator $\hat{K}_{ij}$ given in Eq. (13) preserves the total number of molecules in state $|e\rangle$, but allows a propagation of rotational excitations on the lattice. In the limit of a low number of rotational excitations we diagonalize $\hat{V}_I$ by introducing a set of collective operators $R_{\mathbf{k}}^\dagger$ defined by

$$R_{\mathbf{k}}^\dagger|0_e\rangle\equiv|1_{\mathbf{k}}\rangle=(1/\sqrt{N})\sum_j e^{i\mathbf{k}\mathbf{r}_j^0}|g_1\ldots e_j\ldots g_N\rangle,$$

with a wave vector $\mathbf{k}$ restricted to the first Brillouin zone of the lattice. The operators $R_{\mathbf{k}}$ fulfill (approximate) bosonic commutation relations, $[R_{\mathbf{k}},R_{\mathbf{k}'}^\dagger]\simeq\delta_{\mathbf{k}\mathbf{k}'}$, and in the following we refer to states created by $R_{\mathbf{k}}^\dagger$ as excitons. This nomenclature is based on the similarities of rotational excitations with localized Frenkel excitons in organic crystals [23]. We then identify our qubit state $|1_e\rangle$ as associated with the zero momentum exciton, $R_e^\dagger\equiv R_{\mathbf{k}=0}^\dagger$. Including the energy offset $\hbar\omega_{eg}$ the dynamics of these excitons is given by the Hamiltonian

$$H_{\mathrm{exc}}=\sum_i\hbar\omega_{eg}|e_i\rangle\langle e_i|+\hat{V}_I=\sum_{\mathbf{k}}E(\mathbf{k})R_{\mathbf{k}}^\dagger R_{\mathbf{k}}. \tag{15}$$

The energy band of rotational excitations, $E(\mathbf{k})$, is given in Eq. (21) of Sec. III F where we will discuss it in more detail. For the moment we simply note that Hamiltonian H_{exc} is diagonal in $\mathbf{k}$, such that $[H_{\mathrm{exc}},R_e^\dagger]=E(0)R_e^\dagger$ as already pointed out at the end of Sec. III C.

3. Phonons

In a next step we consider the dynamics of external degrees of freedom of the molecules which is determined by the interaction $\hat{V}_E(\{\mathbf{x}_i\})$ and the kinetic energy $H_{\rm kin}=\Sigma_i \mathbf{p}_i^2/2m$. Since the first-order expansion of $\hat{V}_E(\{\mathbf{x}_i\})$ vanishes due to the definition of equilibrium positions $\mathbf{r}_i^0$, the first nonvanishing contribution is of second order in $\mathbf{x}_i$ and given by

$$\hat{V}_E(\{\mathbf{x}_i\}) = \frac{3\mu_g^2}{16\pi\epsilon_0}\sum_{i\neq j}\frac{5[(\mathbf{x}_i-\mathbf{x}_j)\cdot\mathbf{n}_{ij}^0]^2-[\mathbf{x}_i-\mathbf{x}_j]^2}{|\mathbf{r}_i^0-\mathbf{r}_j^0|^5}. \quad (16)$$

The quadratic interaction between molecules causes collective oscillations (phonons) in the crystal described by the Hamiltonian $H_{\rm phon}=H_{\rm kin}+\hat{V}_E(\{\mathbf{x}_i\})$. As $H_{\rm phon}$ is simply a set of coupled harmonic oscillators it can be written in diagonal form

$$H_{\rm phon} = \sum_{\mathbf{q},\lambda}\hbar\omega_\lambda(\mathbf{q})a_\lambda^\dagger(\mathbf{q})a_\lambda(\mathbf{q}). \quad (17)$$

Here we introduced the annihilation (creation) operators $a_\lambda(\mathbf{q})$ ($a_\lambda^\dagger(\mathbf{q})$) for phonons of quasimomentum $\mathbf{q}$ and frequency $\omega_\lambda(\mathbf{q})$. In 2D, the index λ labels the two different phonon branches. The phonon modes in the dipolar crystal are acoustic phonons. A discussion of the frequency spectrum is given in Sec. III F.

4. Exciton-phonon interactions

The remaining terms of $\hat{V}_{dd}(\{\mathbf{r}_i\})$ which cannot be decomposed into purely internal or external operators are summarized in $\hat{V}_{\rm int}(\{\mathbf{x}_i\})$. The first nonvanishing order of $\hat{V}_{\rm int}(\{\mathbf{x}_i\})$ is linear in the operators $\mathbf{x}_i$ and is given by

$$\hat{V}_{\rm int}(\{\mathbf{x}_i\}) \simeq -\frac{3\mu_g^2}{8\pi\epsilon_0}\sum_{i\neq j}\frac{\mathbf{r}_i^0-\mathbf{r}_j^0}{|\mathbf{r}_i^0-\mathbf{r}_j^0|^5}(\mathbf{x}_i-\mathbf{x}_j)\otimes\hat{K}_{ij}. \quad (18)$$

It describes a state-dependent force on the molecules and entangles internal and external degrees of freedom. In the following we introduce a new symbol $H_{\rm int}\equiv\hat{V}_{\rm int}(\{\mathbf{x}_i\})$ and rewrite Eq. (18) in terms of exciton operators $R_{\mathbf{k}}$ and the phonon operators $a_{\mathbf{q}}$. We obtain an interaction Hamiltonian of the form

$$H_{\rm int} = \sum_{\mathbf{k},\mathbf{q},\lambda} M_\lambda(\mathbf{q},\mathbf{k})[a_\lambda(\mathbf{q})+a_\lambda^\dagger(-\mathbf{q})]R_{\mathbf{k}+\mathbf{q}}^\dagger R_{\mathbf{k}}, \quad (19)$$

which describes scattering processes from state $|\mathbf{k}\rangle$ into state $|\mathbf{k}+\mathbf{q}\rangle$ under the absorption (emission) of a phonon of quasimomentum $\mathbf{q}$ ($-\mathbf{q}$). We postpone a discussion of the explicit form of the coupling matrix elements $M_\lambda(\mathbf{q},\mathbf{k})$ to Sec. III F.

5. Summary

In summary, we have shown that the dynamics of a molecular dipolar crystal given by $H_{\rm MDC}$ in Eq. (5) contains the three contributions,

$$H_{\rm MDC} = H_{\rm exc}+H_{\rm phon}+H_{\rm int},$$

with

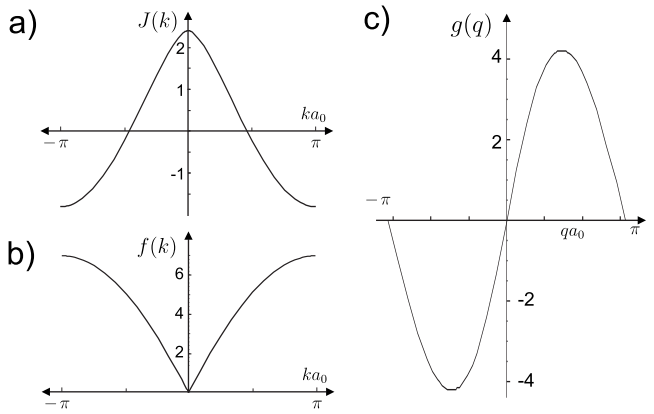

FIG. 3. Dipolar crystal in 1D: (a) Dimensionless band structure $J(k)$ [see Eq. (21)]. (b) Dimensionless phonon spectrum $f(q)$ [see Eq. (23)]. (c) Function $g(q)$ which enters in the expression of coupling matrix elements $M(q,k)$ given in Eq. (25).

$$H_{\rm exc} = \sum_{\mathbf{k}} E(\mathbf{k})R_{\mathbf{k}}^\dagger R_{\mathbf{k}},$$

$$H_{\rm phon} = \sum_{\mathbf{q},\lambda}\hbar\omega_\lambda(\mathbf{q})a_\lambda^\dagger(\mathbf{q})a_\lambda(\mathbf{q}),$$

$$H_{\rm int} = \sum_{\mathbf{k},\mathbf{q},\lambda} M_\lambda(\mathbf{q},\mathbf{k})[a_\lambda(\mathbf{q})+a_\lambda^\dagger(-\mathbf{q})]R_{\mathbf{k}+\mathbf{q}}^\dagger R_{\mathbf{k}}, \quad (20)$$

which is the (minimal) model which describes the evolution of ensemble qubits in a self-assembled molecular dipolar crystal. While explicit expressions for the energy dispersion $E(\mathbf{k})$, the phonon spectrum $\omega_\lambda(\mathbf{q})$, and the scattering matrix elements $M_\lambda(\mathbf{q},\mathbf{k})$ are given in Sec. III F for the 1D and 2D crystal, we first note the general structure of $H_{\rm MDC}$. The ensemble operator $R_e^\dagger$ is an eigenoperator of $H_{\rm exc}$ as well as $H_{\rm phon}$, and therefore, apart form an energy shift, the first two lines of Eq. (20) preserve the coherence of a qubit superposition $|\psi_e\rangle=\alpha|0_e\rangle+\beta|1_e\rangle$. The third line of Eq. (20), $H_{\rm int}$, leads to phonon-assisted transitions from the symmetric qubit state $|1_e\rangle\equiv|\mathbf{k}=0\rangle$ into orthogonal states $|\mathbf{k}\neq 0\rangle$. This loss process is the dominant source of decoherence for a qubit state $|\psi_e\rangle$ and in Sec. III G we calculate the resulting lifetime T_e for the ensemble quantum memory.

F. Molecular dipolar crystals in 1D and 2D

In this section we discuss the exciton dispersion $E(\mathbf{k})$, the phonon spectrum $\omega_\lambda(\mathbf{q})$, and the coupling matrix elements $M_\lambda(\mathbf{q},\mathbf{k})$ which determine the properties of Hamiltonian $H_{\rm MDC}$ given in Eq. (20). For a lattice spacing a_0 we express those quantities in terms of the dipole-dipole energy $U_{dd}=\mu_g^2/(4\pi\epsilon_0 a_0^3)$ and the dimensionless parameters γ, ϵ, and κ. Our focus is placed on the 1D crystal where we derive analytic expressions for the relevant quantities. For the 2D crystal we present numerical results and identify the main differences compared to the 1D case. The derivations of the following results can be found in Appendix A and the main results are summarized in Fig. 3 (1D) and Fig. 4 (2D).

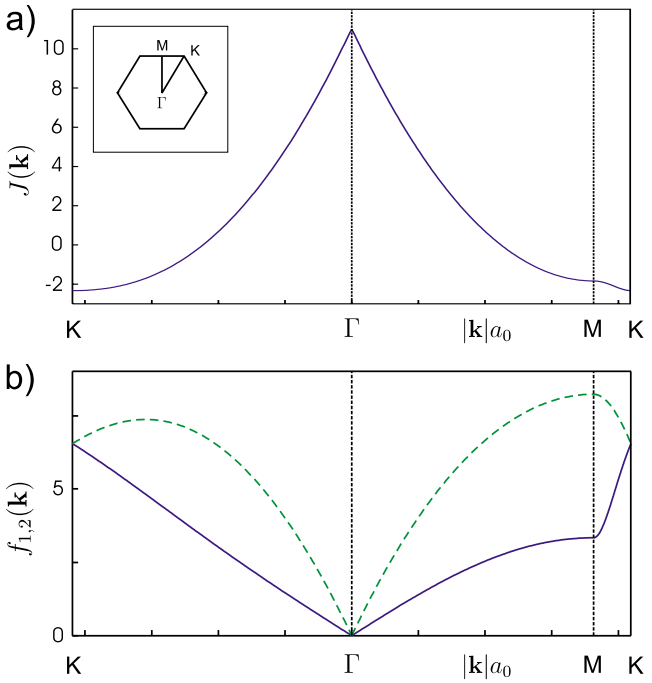

FIG. 4. (Color online) Dipolar crystal in 2D: (a) Dimensionless band structure $J(\mathbf{k})$, [see Eq. (21)]. (b) Dimensionless phonon spectrum $f_\lambda(\mathbf{q})$ [see Eq. (23)]. Band structure and phonon spectrum are plotted for k vectors along the symmetry lines of the first Brillouin zone with symmetry points indicated in the inset of plot (a).

1. Excitons

The energy spectrum of excitons in the dipolar crystal, $E(\mathbf{k})$, contains three contributions,

$$E(\mathbf{k}) = \hbar\omega_{eg} + U_{dd}[\epsilon J(0) + \kappa J(\mathbf{k})], \tag{21}$$

where the dimensionless band structure $J(\mathbf{k})$ is defined in Appendix A in Eq. (A3). While a finite difference in the dipole moments, $\epsilon \neq 0$, only causes a shift of the transition frequency with $J(0)=2\zeta(3)$ in the 1D case and $J(0) \simeq 11.034$ in 2D, the resonant exchange processes proportional to κ lead to the formation of an exciton band structure as shown in Figs. 3 and 4. For the 1D crystal the explicit expression for $J(k)$ is given in Appendix A in Eq. (A4) and we find that in the long-wavelength limit $k \to 0$ it exhibits a nonanalytic behavior,

$$J(k) \simeq J(0) - 3/2[1 - 3/2\ln(ka_0)](ka_0)^2, \tag{22}$$

which is a consequence of the slow decay of dipole-dipole interactions. For the 2D crystal the long-range character of dipole-dipole interactions is even more apparent and results in a linear dispersion $E(\mathbf{k}) - E(0) \sim |\mathbf{k}|$ for small $|\mathbf{k}|$. The total width of the energy band is $\Delta E = 7\zeta[(3)/2]|\kappa|U_{dd}$ in 1D and $\Delta E \simeq 13.37|\kappa|U_{dd}$ in 2D. Note that for rotational states with κ positive, the band structure is "inverted" and the long-wavelength excitations have the highest energy.

2. Phonon spectrum

As shown in Appendix A the spectrum of the acoustic phonon modes in the self-assembled dipolar crystal is of the general from

$$\hbar\omega_\lambda(\mathbf{q}) = \sqrt{\frac{1}{\gamma}} U_{dd} f_\lambda(\mathbf{q}). \tag{23}$$

In the 1D crystal the dimensionless function $f(q)$ defined in Eq. (A8) has a long-wavelength limit $f(q) \simeq \sqrt{12\zeta(3)}qa_0$, and a maximum value of $f(\pi) = \sqrt{93\zeta(5)/2} \simeq 6.94$. The phonon spectrum is therefore characterized by the sound velocity $c = \sqrt{12\zeta(3)/\gamma}a_0 U_{dd}/\hbar$ and the Debye frequency, $\omega_D \equiv \omega(\pi)$,

$$\hbar\omega_D = \sqrt{\frac{93\zeta(5)}{2\gamma}} U_{dd}. \tag{24}$$

The full phonon spectrum is plotted in Fig. 3(b). In the 2D crystal there are two acoustic phonon branches, $\lambda = 1, 2$ and the corresponding dimensionless spectra $f_\lambda(\mathbf{q})$ are plotted in Fig. 4(b). In 2D the maximum phonon frequency is $\hbar\omega_D \simeq 8.22U_{dd}/\sqrt{\gamma}$.

3. Exciton-phonon interactions

Excitons and phonons interact via H_{int} given in the second line of Eq. (20). We write the coupling matrix element as

$$M_\lambda(\mathbf{q},\mathbf{k}) = i\frac{U_{dd}}{\gamma^{1/4}}\sqrt{\frac{1}{Nf_\lambda(\mathbf{q})}}\{\epsilon g_\lambda(\mathbf{q}) + \kappa[g_\lambda(\mathbf{k}+\mathbf{q}) - g_\lambda(\mathbf{k})]\}, \tag{25}$$

where we introduced an additional dimensionless function $g_\lambda(\mathbf{q})$ defined in Appendix A in Eq. (A12). For the 1D crystal the explicit expression of $g(q)$ is given in Eq. (A13) and plotted in Fig. 3(c). The matrix element $M_\lambda(\mathbf{q},\mathbf{k})$ contains two contributions. The first is proportional ϵ and describes a phonon-induced (on-site) energy shift of a molecule in state $|e\rangle$ due to a difference in the induced dipole moments. This type of interaction does only depend on the transferred momentum $\mathbf{q}$ and is familiar from polaron models discussed in solid state physics [24]. The second contribution proportional to κ describes phonon-induced hopping of excitons. The coupling matrix elements for this process also depend on the initial exciton state $|\mathbf{k}\rangle$. In the long-wavelength limit, $|\mathbf{q}| \to 0$, both contributions scales as $\sim\sqrt{|\mathbf{q}|}$, and scattering events with low momentum transfer are suppressed.

Without going into the details of $M_\lambda(\mathbf{q},\mathbf{k})$ we point out two properties which are relevant for the discussion below. First, for long-wavelength excitons the total strength of the exciton-phonon interaction is in the order of

$$|\mathbf{k}| \to 0: \quad O(H_{\text{int}}) = |\epsilon + \kappa| U_{dd}\left(\frac{1}{\gamma}\right)^{1/4}, \tag{26}$$

and therefore only weakly suppressed by the parameter γ. This means that in general the exciton-phonon interaction has a considerable effect on the dynamics of a molecular dipolar crystal even deep in the crystalline phase with $\gamma \gg 1$. However, for a specific choice of rotational states and

values of the electric bias field where $\epsilon+\kappa=0$ is fulfilled, long-wavelength excitons completely decouple from the phonon modes. We come back to this point at the end of Sec. III G.

G. Lifetime of rotational ensemble qubits

Based on the structure of H_{MDC} given in Eq. (20) and the discussion of its properties in Sec. III F, we finally return to the original question of the lifetime of an ensemble qubit prepared in a state $|\psi_e\rangle=\alpha|0_e\rangle+\beta|1_e\rangle$. As already mentioned above we find that the dominant decoherence mechanism arises form the decay of the state $|1_e\rangle$ due to phonon-assisted scattering into orthogonal states $|\mathbf{k}\neq 0\rangle$. This means we can identify the lifetime of the ensemble quantum memory, T_e, with the lifetime of the state $|1_e\rangle$.

1. Ensemble qubit decay

In the following we consider the situation where at some initial time $t=0$ the system is prepared in the state $\rho_0=|0_e\rangle\langle 0_e|\otimes\rho_T$ with ρ_T the equilibrium density operator of the phonon modes for a temperature T. At time $t=0^+$ we instantaneously excite the molecules into the qubit state $|1_e\rangle$ and calculate probability $P_e(t)$ to find the system in state $|1_e\rangle$ after a waiting time t. As we are only interested in times t where $P_e(t)$ is still close to 1, we can use second-order perturbation theory and obtain

$$P_e(t)\simeq 1-\frac{2}{\hbar^2}\int_0^t dt'\int_0^{t'} d\tau\sum_{\mathbf{q},\lambda}|M_\lambda(\mathbf{q},0)|^2\{[N(\omega_\lambda(\mathbf{q}))+1]\times\cos[\Omega^-(\mathbf{q})\tau]+N(\omega_\lambda(\mathbf{q}))\cos[\Omega^+(\mathbf{q})\tau]\}. \quad (27)$$

Here $N(\omega)=1/[\exp(\hbar\omega/k_BT)-1]$ is the thermal occupation number for phonons of frequency ω and $\Omega^{\pm}(\mathbf{q})=[E(0)-E(\mathbf{q})]/\hbar\pm\omega(\mathbf{q})$. For very short times Eq. (27) leads to a quadratic decay of the excited state probability,

$$P_e(t)\simeq 1-W^2t^2, \quad (28)$$

with a characteristic rate W defined by

$$W^2=\frac{1}{\hbar^2}\sum_{\mathbf{q},\lambda}|M_\lambda(\mathbf{q},0)|^2[2N(\omega_\lambda(\mathbf{q}))+1]. \quad (29)$$

For long times the decay of $P_e(t)$ turns into a linear function of t,

$$P_e(t)\simeq 1-\Gamma t, \quad (30)$$

with the decay rate Γ given by Fermi's golden rule,

$$\Gamma=\frac{2\pi}{\hbar^2}\sum_{\mathbf{q},\lambda}|M_\lambda(\mathbf{q},0)|^2\{[N(\omega_\lambda(\mathbf{q}))+1]\delta(\Omega(\mathbf{q})-\omega_\lambda(\mathbf{q}))+N(\omega_\lambda(\mathbf{q}))\delta(\Omega(\mathbf{q})+\omega_\lambda(\mathbf{q}))\}. \quad (31)$$

The crossover time t_c between the quadratic and the linear regime is roughly given by $(t_c)^{-1}\approx\max\{\Delta E/\hbar,\omega_D\}$, with the exciton bandwidth ΔE and the phonon Debye frequency ω_D discussed in Sec. III F. As long as the associated decay probability $P_c=W^2t_c^2$ is much smaller than 1, the application of Fermi's golden rule is valid and we obtain a lifetime $T_e=1/\Gamma$. We refer to this case as the weak coupling regime. Otherwise, for $P_c\approx 1$ or in the strong coupling regime, the qubit decay is determined by the quadratic formula given in Eq. (28) and we identify $T_e=1/W$. At low temperatures we find that when the exciton band width ΔE is larger than $\hbar\omega_D$, $P_c\approx(\epsilon+\kappa)^2/(\kappa^2\sqrt{\gamma})$ while in the opposite case $P_c\approx(\epsilon+\kappa)^2$.

2. Quadratic decay: Strong coupling regime

In the strong coupling regime the initial nonenergy conserving transitions out of the qubit state $|1_e\rangle$ already lead to a strong quadratic reduction of $P_e(t)$. The corresponding rate W defined in Eq. (29) can be written as

$$W^2|_d=\frac{U_{dd}^2}{\hbar^2}\frac{(\epsilon+\kappa)^2}{\sqrt{\gamma}}\mathcal{I}_d\left(\tau=\sqrt{\gamma}\frac{k_BT}{U_{dd}}\right), \quad (32)$$

with $d=1,2$ the dimension of the crystal and $\mathcal{I}_d(\tau)$ a numerical integral

$$\mathcal{I}_d(\tau)=\sum_{\lambda=1}^{d}\int_{\mathrm{BZ}}\frac{d^dq}{V_{\mathrm{BZ}}}\frac{|g_\lambda(\mathbf{q})|^2}{f_\lambda(\mathbf{q})}\left(\frac{2}{e^{f_\lambda(\mathbf{q})/\tau}-1}+1\right). \quad (33)$$

In the two limiting cases this integral behaves as $\mathcal{I}_d(\tau\to\infty)=O(1)$ and $\mathcal{I}_d(\tau\to 0)=O(\tau)$. Neglecting numerical constants arising from the exact evaluation of $\mathcal{I}_d(\tau)$ we can summarize the estimated qubit lifetime T_e as

$$(T_e)^{-1}\approx\frac{U_{dd}}{\hbar}\frac{|\epsilon+\kappa|}{\gamma^{1/4}}\max\{1,\gamma^{1/4}\sqrt{k_bT/U_{dd}}\}. \quad (34)$$

3. Fermi's golden rule: Weak coupling regime

In the weak coupling regime only energy conserved transitions with a certain transferred momentum $\mathbf{q}_0$ lead to the decay of $P_e(t)$. According to Eq. (31) $\mathbf{q}_0$ is defined by $\Omega(\mathbf{q}_0)\pm\omega_\lambda(\mathbf{q}_0)=0$, where the positive (negative) sign applies for a $\kappa<0$ ($\kappa>0$) corresponding to phonon absorption (emission) processes. Based on the discussion on the exciton and phonon spectra given in Sec. III F we distinguish between two cases.

In the first case the resonant k vector is different from zero, $\mathbf{q}_0\neq\mathbf{0}$. Such a situation occurs 1D for $\kappa/\sqrt{\gamma}\gg 1$, when the exciton bandwidth exceeds the phonon bandwidth, $\Delta E\geqslant\hbar\omega_D$. In 2D, due to the linear long-wavelength limit of $E(\mathbf{k})$ this situation occurs only for a negligible parameter regime where $\Delta E\simeq\hbar\omega_D$. The decay rate for 1D is

$$\Gamma_{1\mathrm{D}}=\frac{U_{dd}}{\hbar}\frac{(\epsilon+\kappa)^2}{\kappa\sqrt{\gamma}}C(q_0)[N(\omega(q_0))+\Theta(\kappa)], \quad (35)$$

with $C(q_0)=2g^2(q_0)/[f(q_0)|J'(q_0)+f'(q_0)/\sqrt{\gamma}\kappa|]\lesssim 8$. The Heaviside function $\Theta(\kappa)$ takes into account that only for $\kappa>0$ there is a finite decay rate at $T=0$.

In the second case the resonance condition is only fulfilled for $\mathbf{q}_0=0$. This situation is in general true for a 2D crystal and in 1D for $\kappa/\sqrt{\gamma}<1$. The decay rate then depends on the $|\mathbf{q}|\to 0$ limit of the summand in Eq. (31). As $|M(\mathbf{q},0)|^2\sim|\mathbf{q}|$ vanishes in the long-wavelength limit, we

TABLE I. Different combinations of rotational states $|g\rangle$ and $|e\rangle$ and the corresponding values of $\epsilon=(\mu_e-\mu_g)/\mu_g$ and $\kappa=D_r/\mu_g^2$. States are specified by the quantum numbers $|N,M_N\rangle$ and the value of the external bias field, E_b.

	$\|N,M_N\rangle$	E_b (units of B/μ_0)	μ_g (units of μ_0)	κ	ϵ
(a)	$\|g\rangle=\|1,0\rangle,\|e\rangle=\|2,0\rangle$	3.05	−0.16	10.5	0
(b)	$\|g\rangle=\|1,0\rangle,\|e\rangle=\|3,0\rangle$	3.91	0.09	1	0
(c)	$\|g\rangle=\|0,0\rangle,\|e\rangle=\|1,0\rangle$	8	0.75	0.1	−0.7
(d)	$\|g\rangle=\|0,0\rangle,\|e\rangle=\|1,1\rangle$	5	0.68	−0.24	−0.29
(e)	$\|g\rangle=\|0,0\rangle,\|e\rangle=\|1,0\rangle$	1.44	0.39	1.51	−1.51
(f)	$\|g\rangle=\|1,0\rangle,\|e\rangle=\|3,0\rangle$	3.44	−0.13	0.39	−0.39

only obtain a finite value for Γ in 1D and for a nonzero temperature. The resulting rate is

$$\Gamma_{1D}=(\epsilon+\kappa)^2\sqrt{\frac{3\zeta(3)}{4}}\sqrt{\gamma}\frac{k_BT}{\hbar}. \tag{36}$$

In 2D, due to the additional factor of $|\mathbf{q}|$ in the density of states, we obtain $\Gamma_{2D}=0$.

4. Discussion: Rotational ensemble qubits

In summary we have found that the lifetime T_e of a rotational ensemble quantum memory in a molecular dipolar crystal is primarily determined by the dipole-dipole energy $U_{dd}=\mu_g^2/(4\pi\epsilon_0 a_0^3)$ and depends further on the relation between the dimensionless parameters γ, ϵ, and κ.

For low temperatures the dipole-dipole energy U_{dd} is limited from below by the condition $U_{dd}\geqslant\gamma_c^3\hbar^6/C_3^2m^3$, with γ_c the minimum value of γ which guarantees the stability of the crystal. For an upper bound we use the critical value $\gamma_c=20$ predicted in Refs. [17,21] for the 2D crystal. For the nominal parameters $\mu_g=1$ Debye and $m=100$ amu we obtain $U_{dd}/h\geqslant 260$ kHz. As this bound scales like $\sim 1/\mu_g^4$ choosing molecular states with larger induced dipole moments $\mu_g\sim 5$ D the scale of Γ can in principle be reduced below the kHz regime. However, for a system at finite temperature U_{dd} is also bound from below by k_BT. For a 2D crystal the melting temperature of a dipolar crystal is $T_M\approx 0.09U_{dd}/k_B$ [25], while in 1D we expect a stable crystal for $k_BT\lesssim U_{dd}$ (see Sec. V).

For a given U_{dd} the lifetime of the ensemble qubit depends further on the dimensionless parameters κ and ϵ which in turn depend on the rotational basis states $|g\rangle$ and $|e\rangle$ and the value of the applied bias field E_b. In Table I we have listed a few specific choices of rotational states $|g\rangle$ and $|e\rangle$ and the corresponding values of κ and ϵ. For certain states we find a "sweet spot" of the electric bias field where the induced dipole moments of two rotational states are the same and ϵ vanishes. The value of κ can be significantly reduced by choosing states $|g\rangle$ and $|e\rangle$ with a (to a high degree) dipole-forbidden transition, e.g., $N'=N\pm 2$, with the cost of also lowering the coupling to the microwave cavity. An ideal situation occurs when both ϵ and κ are large but exactly cancel each other, e.g., $\epsilon+\kappa=0$. For such a "magic" configuration the dipole-dipole interactions of the triplet states $|gg\rangle$ and $|ge\rangle+|eg\rangle$ are exactly the same, which makes a symmetric excitation $|1_e\rangle$ insensitive to phonon-induced fluctuations of dipole-dipole interactions. Examples for such phonon-decoupled states are given in rows (e) and (f) of Table I. An additional interesting observation is the absence of energy conserving transitions in a 2D crystal, which in the weak coupling regime implies $\Gamma_{2D}=0$. A detailed investigation of this case and corrections due to higher order terms in the interactions Hamiltonian H_{int} are the subject of future research.

In conclusion we find that the phonon-induced decay of rotational ensemble qubits can cover a wide range of values and is in the end to a large extent determined by the specific experimental implementation of this system. When trapping of molecules can be achieved independent of the rotational state, e.g., in optical or magnetic traps, we can find certain magic configurations in which rotational ensemble qubits are completely decoupled from the phonon bath. In other cases, e.g., for electrostatic traps, we are limited to a certain set of trapped rotational states and typically we are not able to fulfill the decoupling condition $\epsilon+\kappa=0$. In such a situation it is not a good choice to encode quantum information in the rotational degree of freedom.

IV. SPIN-ENSEMBLE QUBITS

In this section we extend our discussion of molecular ensemble qubits to molecules with spin or hyperfine states. This additional internal degree of freedom which is not directly affected by electric dipole-dipole interactions allows us to overcome some of the limitations of purely rotational qubits. In particular, it is then possible to use the rotational degree of freedom to trap molecules in electrostatic potentials and encode quantum information in different spin states, or in contrast to use spin states for magnetic trapping and encode quantum information in rotational degrees of freedom.

A. Rotational spectroscopy of $^2\Sigma$ molecules

In general the rotational spectroscopy of polar molecules involves spin-rotation interactions between the rotation of the nuclei **N** and the spin of unpaired electrons **S** as well as hyperfine interactions between **S** and the nuclear spin **I** [22]. However, to keep the following discussion on a basic level we consider in this paper only the case of a $^2\Sigma$ molecules

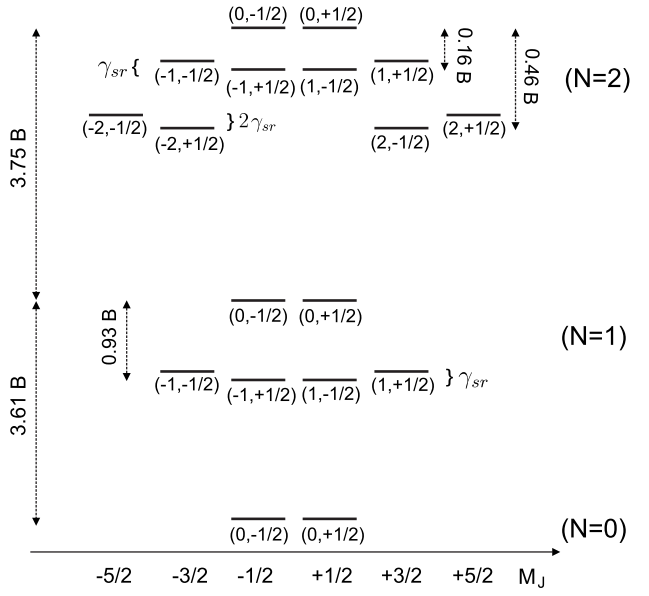

FIG. 5. Spectrum of a $^2\Sigma$ molecule for a bias field $E_b=3.05B/\mu_0$. Eigenstates which are approximately of the form $|N,M_N\rangle_{E_b}\otimes|M_S\rangle$ are individually labeled by (M_N,M_S) while the quantum number N is indicated only for the corresponding manifold.

with a single unpaired electron with spin $S=1/2$ and no nuclear spin $I=0$ for which hyperfine interactions are absent. As, to our knowledge, none of the polar molecules studied in current experiments falls into this category [26], we explain below how the arguments presented for the $^2\Sigma$ molecule can be applied for more complicated molecules with $I>0$ as long as the hyperfine interactions are small compared to the rotational constant B.

In the presence of a bias field $\mathbf{E}_b=E_b\mathbf{e}_z$ the Hamiltonian for a $^2\Sigma$ molecule in the vibrational ground state is

$$H_M = B\mathbf{N}^2 + \gamma_{\rm sr}\mathbf{N}\cdot\mathbf{S} - \mu_z E_b, \tag{37}$$

with $\gamma_{\rm sr}$ the spin-rotation coupling constant, typically in the order of 100 MHz. For a vanishing bias field the spin-rotation coupling lifts the degeneracy of $|N,M_N\rangle_0$ states and new eigenstates of H_M are given by $|N,S;J,M_J\rangle_0$ with $\mathbf{J}=\mathbf{N}+\mathbf{S}$ the total angular momentum. For moderate and strong electric fields $E_b\geqslant B/\mu_0$ the dipole coupling typically exceeds the spin-rotation coupling and eigenstates of H_M are approximately given by product states $|N,M_N\rangle_{E_b}\otimes|M_s\rangle$. Therefore, to a good approximation energy splitting and induced dipole moments are determined by the rotational component only and we refer to the discussion given in Sec. III B. Especially, for states with $M_N=0$ different spin components are degenerate and have exactly the same induced dipole moments. For other values of $M_N\neq 0$ different spin components are split by the spin-rotation coupling, $\sim\gamma_{\rm sr}$, but still have to a good approximation the same induced dipole moments. As an example we plot in Fig. 5 the spectrum of H_M at the "sweet spot" of the bias field, $E_b=E_S\equiv 3.05B/\mu_0$.

For molecules with a finite nuclear spin $I>0$ the physical picture is quite similar although the resulting spectrum is more involved. In the limit of $\gamma_{\rm sr}\to 0$ the hyperfine interaction Hamiltonian $H_{\rm hf}$ couples the electron spin and the nuclear spin to a combined angular momentum $\mathbf{F}_3=\mathbf{S}+\mathbf{I}$ and eigenstates are of the form $|N,M_N\rangle_{E_b}\otimes|F_3,M_{F_3}\rangle$. For a strong electric bias field and for $M_N=0$ this factorized form is approximately conserved even for finite $\gamma_{\rm sr}$ as the spin-rotation coupling is too weak to mix different rotational states. For nonzero M_N the diagonal part of the spin-rotation coupling, $\gamma_{\rm sr}N_zS_z$, does in addition lead to a mixing of different states $|F_3,M_{F_3}\rangle$. This general picture of the spectrum holds as long as $|H_{\rm hf}|,\gamma_{\rm sr}\ll B<\mu_0E_b$ while details depend on the exact relation between hyperfine and spin-rotation coupling.

B. Spin-ensemble qubits in MDC: A protected quantum memory

The additional spin degree of freedom allows us to encode quantum information in ensemble qubits $|0_e\rangle$ and $|1_e\rangle$, where the corresponding molecular basis states $|g\rangle$ and $|e\rangle$ have different spin components. In the following we explain in two examples how the additional spin degree of freedom can, compared to purely rotational states, improve the lifetime of molecular ensemble qubits in a dipolar crystal.

1. Long-lived ensemble quantum memory

We first consider molecular basis states $|g\rangle=|1,0\rangle_{E_b}\otimes|M_S=-1/2\rangle$ and $|e\rangle=|2,0\rangle_{E_b}\otimes|M_S=1/2\rangle$ for the bias field $E_b=E_S$. As we discuss in Sec. V this is an example for two states which can be both trapped in electrostatic fields. The states $|g\rangle$ and $|e\rangle$ have different rotational components and different spin components. At this point it is important to note that the factorization of eigenstates of H_M in a rotational and a spin component is only approximate. The spin-rotation coupling still admixes a small fraction of the other spin component which results in a finite transition dipole matrix element $|\langle e|\boldsymbol{\mu}|g\rangle|$, which actually allows us to couple states $|g\rangle$ and $|e\rangle$ to the microwave cavity. The dimensionless transition matrix element $\Theta_x=|\langle e|\mu_x|g\rangle|/\mu_0$ which determines the coupling to the cavity as well as the parameter κ depends on the ratio $\gamma_{\rm sr}/B$. For the typical case of $\gamma_{\rm sr}\ll B$ we find in numerical calculations $\Theta_x\simeq 2.5(\gamma_{\rm sr}/B)$. For molecules, such as CaBr with $\gamma_{\rm sr}/B=0.03$, the spin-forbidden transition is roughly a factor 7 smaller than the corresponding spin-allowed transition. In contrast, the dimensionless parameter $\kappa\sim\Theta_x^2$ is reduced by a factor $(\gamma_{\rm sr}/B)^2$ and exciton-phonon interactions are strongly suppressed. For our specific example we obtain $\kappa\simeq 250(\gamma_{\rm sr}/B)^2\ll 1$, which should be compared to $\kappa\approx 10$ for spin-conserving transitions [see row (a) in Table I]. Therefore, the spin degree of freedom provides an additional knob to change the interaction parameters κ and ϵ independently and tune the crystal into the weak coupling regime where decay rates are highly reduced (see discussion given in Sec. III G).

2. Protected spin-ensemble quantum memory

To improve the lifetime of the ensemble quantum memory even further we consider in a next step the states $|g\rangle$

$=|1,0\rangle_{E_b}\otimes|M_S=-1/2\rangle$ and $|s\rangle=|1,0\rangle_{E_b}\otimes|M_S=1/2\rangle$. As $|g\rangle$ and $|s\rangle$ have the same rotational component we have introduced the new notation $|s\rangle$ to distinguish this state from the rotationally excited state $|e\rangle$ discussed above. While the states $|g\rangle$ and $|s\rangle$ cannot directly be coupled with a single microwave photon, we can still achieve a coupling to the microwave cavity by a two-photon process involving an additional classical microwave field.

As explained above the two spin states $|g\rangle$ and $|s\rangle$ have the same induced dipole moment, $\epsilon=0$, and in addition there are no resonant dipolar exchange processes between molecules in states $|g\rangle$ and $|s\rangle$ which implies that also $\kappa=0$. Therefore, quantum information encoded in *spin-ensemble qubits* $|0_s\rangle\equiv|0_e\rangle$ and $|1_s\rangle\equiv S_e^\dagger|0_s\rangle=(1/\sqrt{N})\Sigma_i|g_1\ldots s_i\ldots g_N\rangle$ is naturally protected from dipole-dipole interactions and the resulting phonon-induced decay. Higher order spin-flip processes due to virtual excitations into higher rotational states [27,28], which are not included in our model scale as $\sim[\mu_0^4/(16\pi^2\epsilon_0^2a_0^6)]\gamma_{\rm sr}^2/B^3$ and even for $a_0=50$ nm, this rate is only in the order of a few Hz. Therefore, the lifetime of spin-ensemble qubits is mainly limited by the dephasing rate of the spin (or hyperfine states) of a single molecule. Similar to the case of cold atoms [29,30] or trapped ions [31,32] dephasing rates of molecular hyperfine states of below 1 Hz should be achievable.

While highly protected from dipolar interactions spin-ensemble qubits are not directly coupled to microwave photons and the storage and retrieve operations require a two-step process

$$(\alpha|0_c\rangle+\beta|1_c\rangle)\leftrightarrow(\alpha|0_e\rangle+\beta|1_e\rangle)\leftrightarrow(\alpha|0_s\rangle+\beta|1_s\rangle),$$

which involves the rotationally excited ensemble state $|1_e\rangle$. During this process the rotational ensemble qubit is affected by interactions with phonons which cause a decay into orthogonal states $|1_{\mathbf{k}}\rangle$ as discussed in Sec. III G. Therefore, the overall fidelity of an ensemble quantum memory in a MDC is still affected by exciton-phonon interactions. However, by employing a Raman process as discussed in Ref. [2] rotational states are only virtually populated and interactions with phonons are suppressed by the detuning $\Delta=\omega_c-\omega_{eg}$. As we have not yet analyzed the details of the cavity-ensemble coupling we postpone the discussion of gate fidelities to Sec. V D where we study swap operations between microwave photons and spin-ensemble qubits for a specific setup.

V. DIPOLAR CRYSTALS IN A TRAP: INTERFACING MOLECULAR ENSEMBLES AND CIRCUIT QED

In Secs. III and IV we have studied an idealized homogeneous MDC and identified the exciton-phonon interaction as the main source of decoherence for ensemble qubits. We have shown that for certain choices of molecular states, in particular states with a different spin component, phonon-induced decay processes are suppressed and a highly protected ensemble quantum memory can be realized with this system. However, so far we have ignored questions related to the experimental implementation of a MDC, especially questions of transverse and longitudinal trapping potentials. In this section we study the properties of molecular dipolar crystals under realistic experimental conditions, especially in the presence of an additional longitudinal trapping potential.

For a coherent integration of MDCs with a circuit QED system as shown in Fig. 1, trapping of polar molecules close to above the chip surface must not affect coherence properties of the superconducting device. In particular trapping techniques which require the application of strong magnetic fields or intense laser fields raises compatibility questions with high Q-values of superconducting strip line cavities [15]. Therefore, to achieve a strong transverse confinement which is compatible with long coherence times of the microwave cavity, we focus in this paper on a scenario where molecules are trapped by an electrostatic potential as recently proposed in Ref. [1]. In Sec. V A we briefly outline the basic idea of electrostatic trapping of polar molecules and show that this specific trap design will restrict our choice of molecular basis states to a very limited set of rotational states. In Sec. V B we then study the properties of excitons and phonons in a quasi-1D trapping configuration with an additional harmonic confinement potential along the crystal axis. As the confining potential removes the translational symmetry of the crystal, symmetric excitations $|1_e\rangle$ are no longer eigenstates of $H_{\rm exc}$ which opens a new decay channel for rotational ensemble qubits. In Sec. V C we use the spectra of longitudinal and transverse phonon modes to discuss the stability of a 1D crystal in the case of finite temperature and a finite transverse trapping frequency. Finally, in Sec. V D we use these results to discuss state transfer fidelities between a microwave cavity and spin-ensemble qubits under realistic experimental conditions.

A. Electrostatic confinement of polar molecules

In the following we consider a $^2\Sigma$ molecule as discussed in Sec. IV A, in the presence of a bias field $\mathbf{E}_b(\mathbf{r})$ which now depends on the position of the molecule. The Hamiltonian is

$$H_M(\mathbf{r})=B\mathbf{N}^2+\gamma_{\rm sr}\mathbf{N}\cdot\mathbf{S}-\boldsymbol{\mu}\mathbf{E}_b(\mathbf{r}). \tag{38}$$

To achieve trapping we consider an electric field of the form $\mathbf{E}_b(\mathbf{r})=[E_{\rm off}+E_t(\mathbf{r})]\mathbf{e}_z$, with a large offset field $E_{\rm off}$ and a small trapping field $E_t(\mathbf{r})$ with $0\leqslant E_t(\mathbf{r})\ll E_{\rm off}$ and $E_t(\mathbf{r})=0$ at the center of the trap. Without going into the details of the actual trap design we here envision an elongated version of the electric z-trap proposed in Ref. [1] which would produce an electric field configuration of approximately this from.

As long as the position-dependent trapping field $E_t(\mathbf{r})$ is small compared to the offset field $E_{\rm off}$ we can use a Born-Oppenheimer argument and write Hamiltonian (38) as

$$H_M(\mathbf{r})\simeq\sum_n[E_n+V_{t,n}(\mathbf{r})]|n\rangle\langle n|, \tag{39}$$

with $|n\rangle$ (E_n) denoting eigenstates (eigenvalues) of H_M for the bias field $\mathbf{E}_b=E_{\rm off}\mathbf{e}_z$ and $V_{t,n}(\mathbf{r})=-\langle n|\mu_z|n\rangle E_t(\mathbf{r})$. As the electric field has a local minimum at the trap center only weak field seekers with $\mu_n=\langle n|\mu_z|n\rangle<0$ are trapped in this potential. From the discussion in Sec. III B we find that this restriction limits our choice of molecular basis states to states with $M_N=0$ and moderate electric fields.

As indicated by the index n the trapping potential $V_{t,n}$ depends in general on the internal eigenstate $|n\rangle$. In the following we avoid this dependence by tuning the offset field to the "sweet spot," $E_{\text{off}}=E_S$. We choose the two spin states in the $N=1$ manifold, $|g\rangle=|1,0\rangle_{E_S}\otimes|M_S=-1/2\rangle$ and $|s\rangle=|1,0\rangle_{E_S}\otimes|M_S=+1/2\rangle$ as our single molecule basis states for spin-ensemble qubits. Employing a two-photon process the two spin states can be coupled to the microwave cavity via a third, rotationally excited state $|e\rangle=|2,0\rangle_{E_S}\otimes|M_S=-1/2\rangle$. Restricted to those three basis states we can write the molecular Hamiltonian as

$$H_M(\mathbf{r}) \simeq \hbar\omega_{eg}|e\rangle\langle e| + V_t(\mathbf{r}), \tag{40}$$

with $V_t(\mathbf{r})$ a state independent trapping potential for the molecule. Below we consider a quasi-1D trapping configuration with

$$V_t(\mathbf{r}) = \frac{1}{2}m\nu x^2 + \nu_\perp^2(y^2+z^2). \tag{41}$$

Here $\nu_\perp$ is the trapping frequency for the strong transversal confinement and $\nu \ll \nu_\perp$ the trapping frequency for an additional weak confinement along the crystal axis. In this electrostatic trap the transverse trapping frequencies can be as high as $\nu_\perp/2\pi \approx 1-10$ MHz [1].

B. MDC under quasi-1D trapping conditions

In this section we study the properties of a MDC in a quasi-1D trapping configuration where compared to the discussion given for a homogeneous system in Sec. III we add a finite longitudinal and transverse trapping potential $V_t(\mathbf{r})$ as given in Eq. (41). Restricted to the basis states $|g\rangle$, $|s\rangle$, and $|e\rangle$ identified in Sec. V A we extend the crystal Hamiltonian H_{MDC} given in Eq. (5) by the trapping potential $V_t(\mathbf{r})$ and write the total Hamiltonian for the inhomogeneous MDC as

$$H_{\text{MDC}} = \sum_i \left(\frac{\mathbf{p}_i^2}{2m} + V_t(\mathbf{r}_i) + \hbar\omega_{eg}|e_i\rangle\langle e_i| \right) + \hat{V}_{dd}(\{\mathbf{r}_i\}), \tag{42}$$

with the dipole-dipole interaction $\hat{V}_{dd}(\{\mathbf{r}_i\})$ given in Eq. (6). We proceed as in Sec. III and describe dipole-dipole interaction by the induced dipole moment μ_g and the dimensionless operator $\hat{K}_{ij}$. At the "sweet spot" with $\epsilon=0$ the latter is given by

$$\hat{K}_{ij} = \kappa(|g_i,e_j\rangle\langle e_i,g_j| + |e_i,g_j\rangle\langle g_i,e_j|). \tag{43}$$

For our specific choice of rotational states $|g\rangle$ and $|e\rangle$ we find $\kappa \simeq 10.5$ [see Table I, example (a)]. Note that we can omit resonant dipolar interaction between states $|s\rangle$ and $|e\rangle$ as long as most molecules remain in state $|g\rangle$.

Assuming a crystalline phase we replace the molecular position operators by $\mathbf{r}_i=\mathbf{r}_i^0+\mathbf{x}_i$, with $\mathbf{r}_i^0=(x_i^0,0,0)$ and x_i^0 the classical equilibrium position along the crystal axis. As molecules are confined by an additional longitudinal trapping potential the positions x_i^0 are no longer equidistant. In contrast to the discussion given in Sec. III we here also include fluctuations along the transverse directions, e.g., $\mathbf{x}_i=(x_i,y_i,z_i)$, to study the effect of a strong but finite transverse confinement. Expanding H_{MDC} up to the lowest relevant order in $\mathbf{x}_i$ and decompose the crystal Hamiltonian into an exciton part, a phonon part, and exciton-phonon interactions,

$$H_{\text{MDC}} = H_{\text{exc}} + H_{\text{phon}} + H_{\text{int}}. \tag{44}$$

In terms of equilibrium positions x_i^0 the exciton Hamiltonian is given by

$$H_{\text{exc}} = \hbar\omega_{eg}\sum_i |e_i\rangle\langle e_i| + \frac{\mu_g^2}{8\pi\epsilon_0}\sum_{i\neq j}\frac{\hat{K}_{ij}}{|x_i^0-x_j^0|^3}. \tag{45}$$

The phonon Hamiltonian contains now both longitudinal as well as transversal phonons, $H_{\text{phon}}=H_{\text{phon}}^{\parallel}+H_{\text{phon}}^{\perp}$. Primarily we are interested in the longitudinal part which is of the form

$$H_{\text{phon}}^{\parallel} = \sum_j \frac{p_{x,j}^2}{2m} + \frac{1}{2}m\nu^2 x_j^2 + \frac{6\mu_g^2}{8\pi\epsilon_0}\sum_{i\neq j}\frac{(x_i-x_j)^2}{|x_i^0-x_j^0|^5}. \tag{46}$$

Although our focus is placed on the quasi-one-dimensional regime with transverse motion frozen out we include for the moment the Hamiltonian for the transverse phonons, $H_{\text{phon}}^{\perp}$, to study the validity of the quasi-1D approximation. It is given by

$$H_{\text{phon}}^{\perp} = \sum_j \frac{p_{y,j}^2}{2m} + \frac{p_{z,j}^2}{2m} + \frac{1}{2}m\nu_\perp^2(y_j^2+z_j^2) - \frac{3\mu_g^2}{16\pi\epsilon_0}\sum_{i\neq j}\frac{(y_i-y_j)^2+3(z_i-z_j)^2}{|x_i^0-x_j^0|^5}. \tag{47}$$

Note that for fluctuations in the z direction we have included the anisotropy of the dipole-dipole interactions an obtained an additional factor of 3 [see second line of Eq. (47)] which lifts the degeneracy of the two transverse phonon branches.

The leading contribution of H_{int} is linear in the position operators x_i and is given by

$$H_{\text{int}} \simeq -\frac{3\mu_g^2}{8\pi\epsilon_0}\sum_{i\neq j}\frac{x_i^0-x_j^0}{|x_i^0-x_j^0|^5}(x_i-x_j)\otimes\hat{K}_{ij}. \tag{48}$$

Transverse phonons couple to excitons only in second order of y_i and z_i and can be omitted in a first approximation.

Our goal in the following is, to study the properties of excitons and phonons in a MDC in the presence of an additional harmonic confinement potential and compare it with the homogeneous crystal studied in Sec. III. Since for an inhomogeneous system momentum is no longer a good quantum number we introduce a general set of exciton eigenstates,

$$|1_n\rangle \equiv R_n^\dagger|0_e\rangle = \sum_i C_n(i)|g_1\ldots e_i\ldots g_N\rangle, \tag{49}$$

where for $n=1,\ldots,N$ the $C_n(i)$ are the normalized coefficients of the eigenstates of H_{exc} and $R_n^\dagger$ the corresponding set of (approximate) bosonic creation operators. In analogy, we express longitudinal displacement operators x_i in terms of phonon annihilation (creation) operators a_n ($a_n^\dagger$),

$$\hat{x}_i = \sum_{n=1}^{N} \sqrt{\frac{\hbar}{2m\omega(n)}} c_n(i)(a_n + a_n^\dagger), \tag{50}$$

with $c_n(i)$ the mode function for phonons of frequency $\omega(n)$. Ignoring transverse phonons for the moment, the total Hamiltonian for the inhomogeneous dipolar crystal is then of the form

$$H_{\mathrm{MDC}} = \sum_n E(n) R_n^\dagger R_n + \sum_m \hbar\omega(m) a_m^\dagger a_m + \sum_{m,n,n'} M(m,n,n') \times (a_m + a_m^\dagger) R_n^\dagger R_{n'}, \tag{51}$$

and we are left with the evaluation of the exciton spectrum $E(n)$, the phonon spectrum $\omega(m)$, and the coupling matrix elements $M(m,n,n')$. Although in the inhomogeneous case we cannot derive exact analytic expressions for those quantities, good approximate solutions can be found in the limit of large N. The derivations of the following results which are summarized in Appendixes B and C are based on a similar calculation by Morigi *et al.* [33] for the phonon spectrum of a harmonically confined ion crystal.

1. Density profile

In a first step we need to determine the equilibrium positions of N dipoles confined by the harmonic trapping potential, $V_t(x) = m\nu^2 x^2/2$. To do so we define the density $n(x_i^0) = 1/|x_{i+1}^0 - x_i^0|$ which in the limit of large N and a slow variation of the trapping potential becomes a continuous function $n(x)$. In this limit the total potential energy of the crystal is

$$E_{\mathrm{pot}} = \int dx \left(\frac{1}{2} m\nu^2 x^2 - \delta_c \right) n(x) + \zeta(3) C_3 n^4(x), \tag{52}$$

with $C_3 = \mu_g^2/(4\pi\epsilon_0)$ and δ_c the chemical potential to fix the particle number. The energy E_{pot} is minimized for the density

$$n(x) = n(0)\sqrt[3]{1 - 4x^2/L^2}, \tag{53}$$

where the density at the center of the trap $n(0)$ and the length of the crystal, L, are given by

$$n(0) = \frac{\Lambda^{2/5}}{2\zeta(3)^{1/5}} N^{2/5} \sqrt[5]{\frac{m\nu^2}{C_3}}, \tag{54}$$

$$L = \Lambda N a_0, \quad a_0 \equiv n(0)^{-1}. \tag{55}$$

Here we introduced the numerical constant $\Lambda = 5\Gamma(5/6)/[\Gamma(1/3)\sqrt{\pi}] \simeq 1.19$. In Fig. 6 we compare the analytic result for $n(x)$ with a numerical evaluation of the equilibrium positions x_i^0 for molecule numbers up to $N=1000$. We find excellent agreement between numerical and analytic results even for a small number of molecules.

Equations (54) and (55) express the dependence of the center density and the length of the crystal as a function of the molecule number N and a given trapping frequency ν. For comparison with the case of a homogeneous crystal discussed in Sec. III it is more convenient to fix the density at the trap center, $n(0)$, and adjust the trapping frequency ν accordingly. In the following we express quantities in units

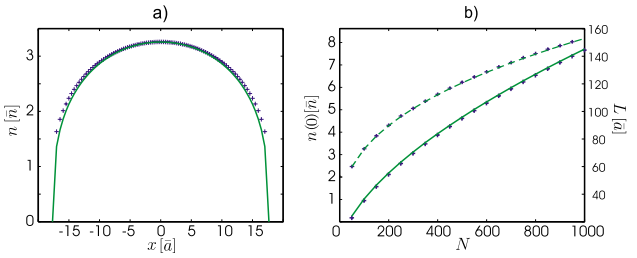

FIG. 6. (Color online) (a) Density profile $n(x)$ for a harmonically confined dipolar crystal for $N=100$ plotted in units of $\bar{a} = (m\nu^2/C_3)^{1/5}$ and $\bar{n} = 1/\bar{a}$. (b) Length L (*solid line*) and center density $n(0)$ (*dashed line*) are plotted as a function of the particle number N. In both figures analytic solutions (*lines*) derived in Sec. V B 1 are compared with numerical calculations (*crosses*).

of $a_0 = 1/n(0)$ and the corresponding energy scale $U_{dd} = \mu_g^2/(4\pi\epsilon_0 a_0^3)$. The dimensionless parameter $\gamma = U_{dd}/(\hbar^2/ma_0^2)$ then gives the ratio between potential and kinetic energy at the *center* of the trap. Note that for a fixed number of molecules we can use the relation

$$2^{-5/2}\sqrt{\gamma\Lambda^2/\zeta(3)}\hbar\nu = U_{dd}/N, \tag{56}$$

to switch between the energy scales of the trapping frequency and the dipole-dipole interaction.

2. Exciton spectrum

Based on a set of equilibrium positions x_i^0 given by the density profile $n(x)$ derived above we now evaluate the energy spectrum of the exciton Hamiltonian H_{exc} (45). As we show in Appendix B in the long-wavelength limit and omitting the energy offset $\hbar\omega_{eg}$ the exciton spectrum has the form

$$\frac{E(n)}{\kappa U_{dd}} \simeq \left[2\zeta(3) - A\sqrt{B_N + \ln\left(\frac{N}{n-1/2}\right)}\frac{n-1/2}{N} \right], \tag{57}$$

with numerical constants $A = 4\sqrt{\zeta(3)}/\Lambda$ and $B_N = 3 + \ln[\Lambda\sqrt{\ln(N/2)/32\zeta(3)}]$.-->--> Similar as for a homogeneous crystal the long-range character of the dipole-dipole interactions leads to logarithmic corrections compared to a harmonic spectrum which would result from nearest-neighbor interactions. The corresponding exciton mode functions $C_n(x)$ are a good approximation given by $C_n(x) \sim \Phi_n(x,\sigma_n)$ with $\Phi_n(x,\sigma_n)$ the standard harmonic oscillator eigenfunctions defined in Eq. (B9) and σ_n a mode-dependent width

$$\sigma_n^2 \simeq N\frac{\Lambda}{4\sqrt{\zeta(3)}}\left[B_N + \ln\left(\frac{N}{n-1/2}\right) \right]^{1/2}. \tag{58}$$

In the short-wavelength limit the exciton energies decrease linearly with increasing n down to a minimum energy $E_{\mathrm{min}} = [-3\zeta(3)/2]\kappa U_{dd}$. The corresponding, rapidly oscillating modefunctions can be written as $C_n(x_i^0) = (-1)\tilde{C}_n(x_i^0)$ with $\tilde{C}_n(x_i^0) \sim \Phi_{N-n+1}(x,\sigma)$ a slowly varying envelope function of width $\sigma \simeq 0.61\sqrt{N}$. Since the fast oscillations in the short-

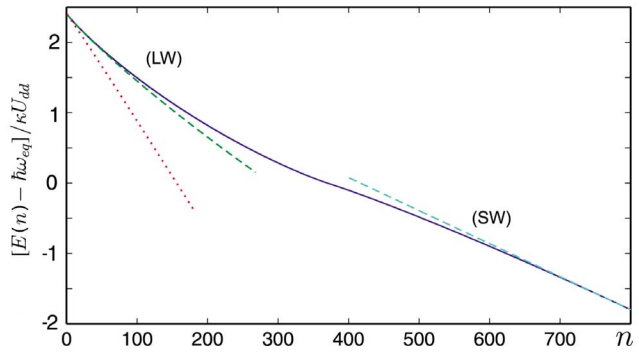

FIG. 7. (Color online) Exciton spectrum $E(n)$ for a harmonically confined MDC for $N=800$ molecules. Numerical results (*solid line*) are compared with analytic approximations derived in Appendix B for the long-wavelength (LW) and short-wavelength (SW) limit (*dashed lines*). The *dotted line* indicates the LW result for the simply harmonic approximation given in Eq. (B10) in Appendix B.

wavelength limit wash out the effect of long-range interactions the spectrum is purely harmonic. The analytic results are compared with a numerical diagonalization of $H_{\rm exc}$ in Fig. 7. Note that the total width of the exciton spectrum, $\Delta E=7\zeta(3)\kappa U_{dd}/4$ is exactly the same as in the homogeneous case. This is due to the fact that both long- and short-wavelength excitons are located at the center of the trap where the density is almost constant.

3. Phonon spectrum

The phonon spectrum of a quasi-1D MDC with a strong transverse trapping frequency $\nu_\perp$ and a weak longitudinal trapping frequency ν consists of one longitudinal ("acoustic") and two transverse ("optical") phonon branches which are plotted in Fig. 8. In Appendix C we derive approximate analytic expressions for the long- and short-wavelength limits of the individual branches. For the moment we restrict our discussion to the longitudinal modes and come back to some properties of transverse phonons in Sec. V C.

In the long-wavelength limit the spectrum of longitudinal phonons determined by $H^{\parallel}_{\rm phon}$ defined in Eq. (46) is of the form

$$\omega(m) \simeq \nu\sqrt{1+(3m^2-m-2)/2}. \tag{59}$$

We recover the exact results for the center of mass mode $\omega(1)=\nu$ and the breathing mode $\omega(2)=\sqrt{5}\nu$ and obtain a roughly linear phonon spectrum $\omega(m)\simeq\nu 1.22m$ for larger m. The corresponding mode functions $c_m(i)$ describe collective oscillations extended over the whole crystal.

In the short-wavelength limit the spectrum of longitudinal phonons is given by

$$\omega(m)=\omega_D\left(1-\sqrt{\frac{40\zeta(3)}{31\zeta(5)\Lambda^2}}\frac{(\bar{m}+1/2)}{N}\right), \tag{60}$$

with $\bar{m}=N-m$ and a Debye frequency $\omega_D=\nu N\Lambda\sqrt{93\zeta(5)/64\zeta(3)}$. When we reexpress the Debye frequency in units of U_{dd} using Eq. (56) we find that ω_D exactly matches the Debye frequency of a homogeneous crystal

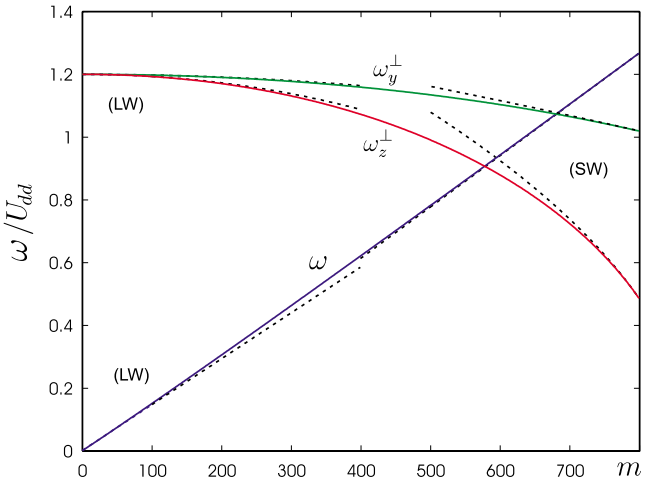

FIG. 8. (Color online) Phonon spectrum of a harmonically confined MDC under quasi-1D trapping conditions for $N=800$ molecules. The solid lines show the numerically evaluated spectrum for longitudinal (ω) and transverse ($\omega^\perp_{y,z}$) phonons in units of U_{dd} and for $\gamma=30$ and $\hbar\nu_\perp/U_{dd}=1.2$. The dashed lines show the analytic results derived in Appendix C for the long-wavelength (LW) and short-wavelength (SW) limits of the three different branches.

given in Eq. (24). This apparent coincident is based on the fact that in the short-wavelength limit phonon mode functions are of the form $c_m(i)\approx(-1)^i\tilde{c}_{\bar{m}}(i)$, with an envelope function $\tilde{c}_{\bar{m}}(i)$ that is localized at the center of the trap [see Eq. (C9) in Appendix C], and is therefore not sensitive to the variation of the density at the edges of the crystal.

In summary we find that the longitudinal phonon spectrum of a harmonically confined MDC is to good approximation linear and it is hardly affected by the long-range character of dipole-dipole interactions. The numerical results plotted in Fig. 8 agree well with our analytic expressions given in Eqs. (59) and (60) and show that for most purposes we can simply approximate the spectrum by $\omega(m)\simeq\omega_D m/N$ where the Debye frequency ω_D is the same as in a homogeneous crystal of density $n=n(0)$.

4. Exciton-phonon interaction

The exciton-phonon interaction Hamiltonian $H_{\rm int}$ defined in Eq. (48) describes transitions between excitons in mode $C_n(i)$ and $C_{n'}(i)$ by simultaneously emitting or absorbing phonons in mode $c_m(i)$. Due to the absence of momentum conservation for a dipolar crystal in a trap, the transition matrix element $M(m,n,n')$ for this process depends on all three indices and has a more complicated structure as in the homogeneous case. Using the approximate phonon spectrum $\omega(m)\simeq\omega_D m/N$ with ω_D given in Eq. (24) we can write transition matrix elements as

$$M(m,n,n')=-\frac{\kappa U_D}{\gamma^{1/4}}\mathcal{M}(m,n,n'), \tag{61}$$

where in terms of normalized equilibrium positions $\bar{x}_i^0=x_i^0/a_0$ the dimensionless matrix element is

$$\mathcal{M}(m,n,n') = \sqrt[4]{\frac{27}{62\zeta(5)}}\sqrt{\frac{N}{m}}\frac{1}{2}\sum_{i\neq j}\frac{\bar{x}_i^0 - \bar{x}_j^0}{|\bar{x}_i^0 - \bar{x}_j^0|^5}[c_m(i) - c_m(j)] \times [C_{n'}(i)C_n(j) + C_{n'}(j)C_n(i)]. \quad (62)$$

By replacing the coefficients $C_n(i)$ $[c_m(i)]$ by the continuous mode functions $C_n(x)$ $[c_m(x)]$ derived in Appendixes B and C it is possible to study some general properties for the matrix elements $M(m,n,n')$. For example, for long-wavelength phonons $(m/N \ll 1)$ we find $c_m(i) - c_m(j) \sim c'_m(x_i^0) \sim m/N$ and recover the scaling $M(m,n,n') \sim \sqrt{m/N}$ in analogy to the homogeneous crystal. We here do not go further into analytic details of $M(m,n,n')$ and instead we use in our calculations below numerically evaluated values for $\mathcal{M}(m,n,n')$.

C. Stability of the crystalline phase

Our analysis so far has been based on the assumption that the molecules form a linear crystal with small fluctuations around equilibrium positions. This assumption is valid in the limit of $\gamma \gg 1$, low temperatures, $k_b T \ll U_{dd}$, and strong transverse confinement $\hbar\nu_\perp \gg U_{dd}$. Since in a real experiment none of these conditions is strictly satisfied we now study the stability of our system for finite values of γ, T, $\nu_\perp$. We identify three processes which destabilize the dipolar crystal. First, longitudinal fluctuations of the molecules eventually lead to a melting of the crystalline structure. For $T=0$ and a homogeneous system this crossover has been studied numerically in Refs. [19,20], but we are not aware of similar studies for finite T or for finite trapping potential. Second, for a weak transverse confinement there is a regime where the linear chain is no longer the correct ground state and molecules order in a zig-zag configuration. This so-called "zig-zag instability" is well known for a linear chain of trapped ions where it has been analyzed theoretically [33–35] and verified experimentally [36]. A third process which has been studied in Refs. [17,18] is quantum tunneling of molecules into regions where dipole-dipole interactions are attractive.

1. Longitudinal stability of a dipolar crystal

We first study the melting of a dipolar crystal due to longitudinal quantum and thermal fluctuations of the molecules. A rigorous treatment of this problem would in principle require to take into account the full quantum many-body theory for our 1D dipolar system which is beyond the scope of the present work. Instead we here present a much simpler calculation assuming the validity of the phonon Hamiltonian $H_{\text{phon}}^{\parallel}$ and determine the parameter regime where our model is self-consistent, i.e., where fluctuations are small compared to the mean separation of the molecules.

To study local fluctuations of the molecules in the presence of a longitudinal trapping potential we introduce the position-dependent Lindemann parameter

$$\Gamma_L(x,T) = n(x)\Delta_x(x,T), \quad (63)$$

with $(\Delta_x)^2(x_i^0,T) = \langle (x_{i+1} - x_i)^2 \rangle$ and the average is taken with respect to the phonon equilibrium density operator at temperature T. By employing the sound wave approximation $\omega(m) = \omega_D m/N$ we can write $\Gamma_L(x,T)$ as

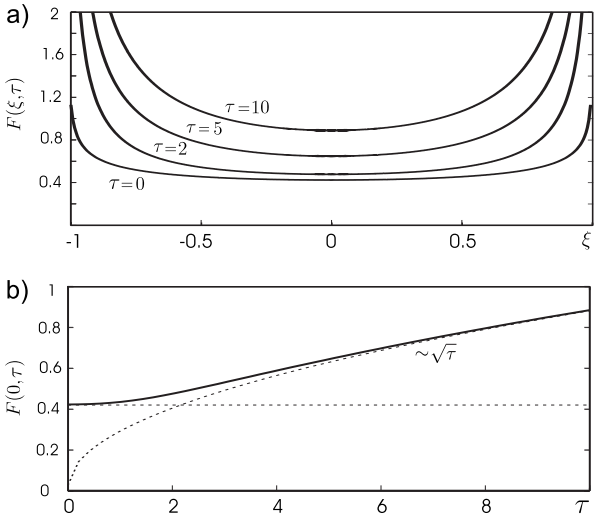

FIG. 9. Numerical results for the function $F(\xi,\tau)$ introduced in Eq. (64) for $N=800$. (a) $F(\xi,\tau)$ is plotted as a function of $\xi = 2x/L$ for different values of $\tau = \sqrt{\gamma} k_B T/U_{dd}$. (b) $F_h(\tau) \equiv F(\xi = 0,\tau)$ is plotted as a function of τ (solid line). The two dashed lines indicate the two limits $F_h(\tau \ll 1) \simeq 0.42$ and $F_h(\tau \gg 1) \simeq 0.28\sqrt{\tau}$. See text for more details.

$$\Gamma_L(x,T) = \left(\frac{1}{\gamma}\right)^{1/4} F\left(\xi = \frac{2x}{L}, \tau = \sqrt{\gamma}\frac{k_B T}{U_{dd}}\right), \quad (64)$$

with a universal function $F(\xi,\tau)$ defined in Appendix D in Eq. (D4). In Fig. 9 we plot the dependence of $F(\xi,\tau)$ on temperature and position. For the homogeneous crystal we obtain an analogous result with $F(\xi,\tau)$ in Eq. (64) replaced by $F_h(\tau)$. Due to the nearly constant density at the center of the trap we identify $F_h(\tau) \equiv F(\xi = 0,\tau)$. From Eq. (64) we find that fluctuations are only weakly suppressed with increasing γ which is already reflected in the $\gamma^{-1/4}$ dependence of the exciton-phonon interaction [see Eq. (26)].

The minimal criterion for the local stability of the crystalline phase and therefore the self-consistency of our model is $\Gamma_L(x,T) \leq 1$. To improve this criterion we argue as follows. By quantum Monte Carlo simulations it has been predicted [19,20] that at $T=0$ a crystalline phase appears for $\gamma > \gamma_c \approx 1$, or in terms of our Lindemann parameter $\Gamma_L(0,0) \leq F(0,0)/\gamma_c^{1/4} \simeq 0.42$. It is reasonable to assume that a generalization of this criterion, $\Gamma_L(x,T) \leq 0.42$, should also provide a good estimate for the local existence of a crystalline phase for a finite temperature and for an inhomogeneous density profile. Note that for the parameter regime $\gamma \approx 10$–100 this criterion translates into $F(\xi,\tau) \leq 0.42\gamma^{1/4} \approx 1$. From Fig. 9(a) we find that for $\tau = 0$ fluctuations in the crystal are roughly constant and almost the whole crystal is in a crystalline phase. For $\tau > 0$ fluctuations at the edges of the chain quickly start to increase and at around $\tau \approx 5$–10 already a significant fraction of the system does not fulfill stability criterion. Therefore for the inhomogeneous crystal we deduce the temperature limit $k_B T \lesssim 5U_{dd}/\sqrt{\gamma}$. For the homogenous crystal we find $F_h(\tau \gg 1) \simeq 0.28\sqrt{\tau}$ (see Appendix

D) which leads to a similar limit for the temperature of $k_bT \lesssim 2.4U_{dd}$.

2. Transverse stability of a dipolar crystal

Position fluctuations of the molecules in transverse directions are described by the Hamiltonian $H^{\perp}_{\text{phon}}$ given in Eq. (47). The resulting phonon spectrum of the two transverse phonon branches is plotted in Fig. 8 and approximate analytic expressions for the long- and short-wavelength limit can be found in Appendix C in Eqs. (C11) and (C12). As transverse phonons are hardly influenced by the longitudinal trapping potential we use in the following discussion the exact spectrum of transverse phonons in a homogeneous crystal, which can be written in a closed form as

$$\omega^{\perp}_{y,z}(q) = \sqrt{\nu_{\perp}^2 - \frac{\alpha_{y,z}}{4\gamma}\left(\frac{U_{dd}}{\hbar}\right)^2 f^2(q)}. \tag{65}$$

Here $\alpha_y=1$, $\alpha_z=3$ and $f(q)$ is given in Eq. (A8). From Eq. (65) we see that transversal phonons are "optical" phonons with a offset frequency $\nu_{\perp}$ and in the quasi-1D limit, $\hbar\nu \gg U_{dd}$ they form a flat band, $\omega^{\perp}_{y,z}(q) \approx \nu_{\perp}$. However, when $\hbar\nu_{\perp}$ and the dipole-dipole interaction U_{dd} are of the same order we find a significant reduction of $\omega^{\perp}_{x,y}(q)$ for short-wavelength phonons (see Fig. 8). In particular the transverse phonons along the z direction reach a minimum frequency of

$$\omega^{\perp}_{\text{min}} = \sqrt{\nu_{\perp}^2 - \frac{279\zeta(5)}{8\gamma}\left(\frac{U_{dd}}{\hbar}\right)^2}. \tag{66}$$

The meaning of $\omega^{\perp}_{\text{min}} \to 0$ is that the linear chain of molecules becomes a metastable configuration and a new ground state appears where molecules are ordered in a "zig-zag" configuration. To avoid this "zig-zag" instability the minimum requirement for the transverse confinement frequency is

$$\hbar\nu_{\perp} > 6.08U_{dd}/\sqrt{\gamma}. \tag{67}$$

While the "zig-zag" instability is a purely classical effect there is also a quantum mechanical instability of a quasi-1D dipolar crystal due to tunneling events into the region of attractive dipole-dipole interactions. For a detailed description of this process the reader is referred to Ref. [18] where this tunneling rate has been analyzed for the case of two molecules approaching each other under 1D or 2D trapping conditions. When we adopt the result derived in Ref. [18], Sec. III A 4, and use ω_D as the attempt frequency we obtain tunneling rate

$$\Gamma_{\text{tun}} \simeq \omega_D \exp[-c\sqrt[5]{\gamma^3\hbar\nu_{\perp}/(8U_{dd})}], \tag{68}$$

with a numerical constant $c \approx 5.8$. When we assume that the inequality (67) is satisfied we find that the tunneling rate is bound from above by $\Gamma_{\text{tun}} \lesssim \omega_D \exp(-c\sqrt{\gamma})$. We conclude that when the system is in a crystalline regime, $\gamma > 1$, and condition (67) is fulfilled, the crystal is also stable with respect to tunneling events.

3. Summary

In summary we find that apart from $\gamma > 1$ the stability of a homogeneous quasi-1D dipolar crystal requires the following relation between the relevant energy scales:

$$\max\left(\frac{\hbar^2}{ma_0^2}, 0.42k_BT\right) < U_{dd} < \sqrt{\gamma}\frac{\hbar\nu_{\perp}}{6.08}. \tag{69}$$

In the inhomogeneous case the bound on the temperature should be replaced by $k_BT \lesssim 5U_{dd}/\sqrt{\gamma}$ to guarantee a crystalline structure over a large fraction of the system. Finally we emphasize that numerical values for the bound on the temperature should not be considered as precise numbers. On the one hand, this is due to our simplified model that we used to calculate these numbers. On the other hand, in a 1D configuration we expect a smooth crossover from a crystalline to a liquid regime with no precisely defined transition point. In that sense Eq. (69) determines the parameter regime where our model Hamiltonian H_{MDC} (51) is valid. Outside this regime we do not expect a complete breakdown of our model but higher order corrections should be taken into account.

D. State transfer fidelities for spin-ensemble qubits

So far in Sec. V we have discussed several aspects of a MDC in the presence of a finite longitudinal and transverse confinement potential and we have identified the stability criteria for such a system. In particular we have focused on a specific scenario where molecules are trapped in electrostatic potentials which provides a convenient way to achieve strong transverse confinement and the possibility to bring molecules close to the surface of the cavity electrode to enhance the coupling strength. However, the severe restriction on trapping rotational states limits the induced dipole moments to $\mu_g \approx 0.2\mu_0 \approx 1$ D while at the same time resonant dipole-dipole interaction and therefore exciton-phonon interactions are quite large ($\kappa \approx 10$). In this section we finally show that even under those unfavorable conditions we may still achieve high-fidelity state transfer operations between the cavity and ensemble qubits encoded in collective spin excitations.

1. Ensemble-cavity coupling

In order to couple the two spin states $|g\rangle$ and $|s\rangle$ defined in Sec. V A we consider a Raman type setup where $|g\rangle$ and the rotational state $|e\rangle$ are coupled to the cavity field and $|e\rangle$ is in turn coupled to state $|s\rangle$ by a classical microwave field of orthogonal polarization. For this configuration the cavity-molecule interaction is

$$H_{\text{cav-mol}}(t) = \sum_i g(x)|g_i\rangle\langle e_i|c^{\dagger} + \frac{\Omega(t)}{2}|s_i\rangle\langle e_i| + \text{H.c.}, \tag{70}$$

with $\Omega(t)$ the controllable Rabi frequency of the external microwave field. In Eq. (70) we have generalized our model to a nonuniform cavity mode function by introducing the position-dependent single molecule coupling $g(x)=gu(x)$. Here g is the maximum coupling constant at the center of the trap and $0 \leq u(x) \leq 1$. Note that $u(x)$ varies at least on the scale of the cavity wavelength λ_c, but may in principle be designed to have an arbitrary shape. Under the two-photon

resonance condition and a detuning $\Delta=\omega_c-\omega_{eg}\gg g\sqrt{N},\Omega(t)$ we can eliminate the excited state and obtain

$$H_{\text{cav-mol}}(t)=g_R(t)(S_e^\dagger c+c^\dagger S_e), \tag{71}$$

with a Raman coupling strength $g_R(t)=g_N\Omega(t)/2\Delta$. Note that due to the nonuniform cavity-molecule coupling we obtain a modified ensemble coupling $g_N\equiv g\sqrt{N_{\text{eff}}}$ with an effective number of molecules $N_{\text{eff}}=\int|u(x)|^2n(x)dx$. Similarly, ensemble qubit states are defined as

$$|1_s\rangle\equiv S_e^\dagger|0_s\rangle=\frac{1}{\sqrt{N_{\text{eff}}}}\sum_i u(x_i^0)|g_1\ldots s_i\ldots g_n\rangle. \tag{72}$$

Assuming for simplicity $\Omega(t)/2\approx g_N$ the Raman coupling Hamiltonian (71) provides the basic ingredient for a swap operation between the state of the cavity and the spin-ensemble qubit in a time $T_S=\pi\Delta/2g_N^2\sim 1/g_N$. For a realistic estimate of g_N we consider the predictions for the single molecule coupling strength g which are given in Ref. [1] for CaBr with $\mu_0=4.3$ D. With d the distance between the molecules and the cavity electrode we obtain

$$g_N/(2\pi)\simeq 40\text{ kHz}\times\sqrt{N_{\text{eff}}}/d\ \mu\text{m}. \tag{73}$$

As in the crystalline phase we do not have to care about motional diffusion of molecules the length of the crystal can in principle be as large as $L\approx\lambda_c/2$ meaning that even for a 1D crystal the number of molecules can be as high as $N_{\text{eff}}\approx\lambda_c/(2\Lambda a_0)\approx 10^5$. Using a moderate trap distance $d=0.5\ \mu$m we end up with a collective coupling strength in the order of $g_N/(2\pi)\approx 25$ MHz, which can in principle be pushed into the 100 MHz regime by going to trap-surface distances of $d\approx 0.1\ \mu$m.

2. Decay of rotational ensemble qubits

As decoherence processes for spin-ensemble qubits during gate operations are due to a finite population of the rotationally excited state $|e\rangle$ we study in a first step the decay of a rotational ensemble qubit state $|1_e\rangle$. Following the calculations of Sec. III G the initial decay of the excited state probability is $P_e(t)\approx 1-W^2t^2$, where compared to the homogeneous case the decay rate W now contains two contributions,

$$W^2=\left(\frac{\kappa U_{dd}}{\hbar}\right)^2\left(\mathcal{I}_{\text{exc}}+\frac{\mathcal{I}_{\text{phon}}}{\sqrt{\gamma}}\right). \tag{74}$$

The first term in Eq. (74) is the exciton dispersion which arises in an inhomogeneous system from the mismatch between cavity modefunction and exciton eigenfunctions. In terms of the normalized exciton spectrum $\bar{E}(n)=[E(n)-\hbar\omega_{eg}]/(\kappa U_{dd})$ and the overlap $z_n=\Sigma_i C_n(i)u(x_i^0)$ it is given by

$$\mathcal{I}_{\text{exc}}=\sum_n\bar{E}^2(n)z_n^2-\left(\sum_n\bar{E}(n)z_n^2\right)^2. \tag{75}$$

For a cavity mode function $u(x)=\cos(\pi x/\lambda_c)$ and $L\leqslant\lambda_c/2$ we obtain numerical values of $\mathcal{I}_{\text{exc}}\simeq 0.40-0.11$, where the lower value corresponds to $L=\lambda_c/2$. Of course, a more sophisticated trap or cavity design would reduce this value even further toward $\mathcal{I}_{\text{exc}}\simeq 0$, e.g., in the limit of a flat bottom trap.

The second term in Eq. (74) describes the decay due to exciton-phonon interactions and is defined as

$$\mathcal{I}_{\text{phon}}=\sum_{m,n,n'}z_nz_{n'}|\mathcal{M}(m,n,n')|^2[2N(\omega(m))+1], \tag{76}$$

with normalized coupling matrix elements $\mathcal{M}(m,n,n')$ defined in Eq. (62). A numerical evaluation of $\mathcal{I}_{\text{phon}}$ for the case $L\ll\lambda_c$ shows that in the zero temperature limit $\mathcal{I}_{\text{phon}}\approx 1.38$ while for high temperatures we obtain $\mathcal{I}_{\text{phon}}\approx 11.3\tau$, with $\tau=\sqrt{\gamma}k_BT/U_{dd}$. The crossover point between the two regimes is $\tau\approx 1$.

3. State transfer fidelities for spin-ensemble qubits

For a simplified discussion of the state transfer fidelity between the microwave cavity and spin-ensemble qubits we identify the gate fidelity $\mathcal{F}$ with the probability to convert a single cavity photon, $|1_c\rangle$, into a spin excitation $|1_s\rangle$. The fidelity is degraded by two processes. First, the spin state $|1_s\rangle$ decays due to the finite admixture of the rotational ensemble state $|1_e\rangle$. For a detuning $\Delta\gg|H_{\text{MDC}}|$ and the fast gate times T_G considered in this paper this decay is quadratic and the corresponding rate $W_s\approx(g_N/\Delta)^2W$ is proportional to W defined in Eq. (74), but suppressed by $(g_N/\Delta)^2$. Second, the photon state $|1_c\rangle$ decays linearly with the cavity decay rate Γ_c. Assuming that each of the two processes acts for approximately one-half of the gate time T_G, we obtain a total gate fidelity

$$\mathcal{F}\simeq 1-\left(\frac{\pi W}{4\Delta}\right)^2-\frac{\pi\Gamma_c\Delta}{4g_N^2}. \tag{77}$$

We optimize the gate fidelity for a detuning $\Delta_*=(\pi g_N^2W^2/\Gamma_c)^{1/3}$ which results in a maximal fidelity of

$$\mathcal{F}_*\simeq 1-\frac{3}{4}\left(\frac{\pi}{2}\right)^{4/3}\left(\frac{\Gamma_cW}{g_N^2}\right)^{2/3}. \tag{78}$$

Discussion. We now consider a specific example using the molecule CaBr with $\mu_0=4.3$ D, $m=120$ amu, and $B/2\pi=2.8$ GHz. From (a) in Table I, we find that at the sweet spot the induced dipole moment is $\mu_g\approx 0.7$ D and $\kappa=10.5$. To achieve a stable crystal we choose a lattice spacing of $a_0=70$ nm which corresponds to $\gamma\approx 13$ and $U_{dd}/(2\pi)=215$ kHz. From our estimates on the stability of the crystal in Sec. V C we obtain the conditions $k_BT\lesssim 2U_{dd}\approx 20\ \mu$K and $\nu_\perp/2\pi>360$ kHz. Both requirements seem feasible with on-chip cooling and trapping techniques proposed in Ref. [1]. Trapping a moderate number of molecules $N\approx 10^4$ at a distance $d\approx 0.5\ \mu$m above the cavity electrode we obtain a collective coupling strength of $g_N/2\pi\approx 8$ MHz. Using a superconducting microwave cavity with a quality factor $Q\approx 10^6$ as demonstrated in Ref. [15] the decay rate of the cavity is as low as $\Gamma_c=\omega_c/Q\approx 2\pi\times 10$ kHz. Without any mode matching but assuming temperatures of $k_BT\leqslant U_{dd}/\sqrt{\gamma}\approx 3\ \mu$K we obtain $W/(2\pi)\approx 2$ MHz. Inserting these values into Eq. (78) we obtain a gate fidelity of $F\simeq 0.994$ and a gate time of $T_G\approx 0.14\ \mu$s. For a more opti-

mistic choice of parameters with $g_N/2\pi=25$ MHz and $a_0=100$ nm (which corresponds to $\gamma\approx 9$, $U_{dd}/2\pi\approx 75$ kHz and a temperature requirement $k_BT<1$ μK) we immediately obtain gate errors of below 10^{-3} at even shorter gate times.

In conclusion we find that while in an electrostatic trapping configuration exciton-phonon interactions are quite high, it can be overcome by the high collective coupling strength due to the high densities in the crystalline phase and the low trap surface distance. However, for further improvements it might be necessary to consider magnetic trapping techniques where exciton-phonon interactions can be highly reduced while at the same time temperature requirements would be less stringent. A second interesting alternative is the choice of rotational states $|g\rangle$ and $|e\rangle$ which are given in Table I, example (e). Both states are weak field seekers *and* at the same time they satisfy the decoupling condition $\kappa+\epsilon=0$. However, as molecules in state $|g\rangle$ and $|e\rangle$ have a different induced dipole moment and feel a different trapping potential, this configuration would require a flat bottom trap in longitudinal direction and ground state cooling in transverse directions.

VI. SUMMARY AND CONCLUSION

In this paper we have investigated the storage of quantum information encoded in collective excitations (ensemble qubits) of long-lived rotational or spin degrees of freedom in a self-assembled dipolar crystal of polar molecules. This provides a high-fidelity quantum memory which can be coupled to a superconducting strip line cavity which in the spirit of cavity QED provides a coupling to a solid state quantum processor. The main results are summarized as follows.

In the first part of this work we have studied the dynamics of rotational excitations (=excitons) in a self-assembled molecular dipolar crystal (MDC) which maps to a polaron-type model with excitons interacting with the phonon modes of the crystal. While in general the exciton-phonon interactions plays the dominant role as a decoherence mechanism in this system, leading to a decay of rotational ensemble qubits, we have identified certain "magic" configurations where long-wavelength excitons—which includes the ensemble qubit state—decouple from the phonon modes. Furthermore, quantum information encoded in spin-ensemble qubits is naturally protected from dipole-dipole interactions, and the exciton-phonon interactions affects the ensemble quantum memory only during gate operations.

In the second part of this paper we have studied in detail a specific scenario with molecules trapped in electrostatic potentials (e.g., an on-chip electric trap) and quantum information encoded in collective spin excitations. We have discussed modification of the exciton and phonon spectrum due to the presence of a longitudinal trapping potential and analyzed the stability of a MDC in a quasi-1D geometry. An estimate of the expected state transfer fidelities between the microwave cavity and spin-ensemble qubit for this setup shows that under reasonable experimental conditions fidelities of $\mathcal{F}\geqslant 0.99$ can be achieved for a total gate time well below 1 μs. Optimized conditions would result in gate errors of $\sim 10^{-4}$ which would allow fault tolerant quantum computing [37]. This specific example demonstrates the potential of MDCs in the context of hybrid quantum computing since high gate fidelities and long storage times are combined with gate times that are compatible with decoherence times scales in solid state based quantum computing.

ACKNOWLEDGMENTS

The authors thank H. P. Büchler, A. Micheli, G. Pupillo, and M. Lukin for stimulating discussions and P. Xue for contributions at the initial stage of this work. This work was supported by the Austrian Science Foundation (FWF), the European Union projects EuroSQIP (Contract No. IST-3-015708-IP), CONQUEST (Contract No. MRTN-CT-2003-505089), SCALA (Contract No. IST-15714), and the Institute for Quantum Information.

APPENDIX A: HOMOGENEOUS DIPOLAR CRYSTAL

In this appendix we briefly summarize the derivation of the exciton spectrum $E(\mathbf{k})$, the phonon spectrum $\omega_\lambda(\mathbf{k})$, and the coupling matrix elements $M_\lambda(\mathbf{q},\mathbf{k})$ for a homogeneous dipolar crystal in 1D and 2D. All results in this appendix are expressed in units of the lattice spacing a_0 and the corresponding dipole-dipole energy $U_{dd}=\mu_g^2/(4\pi\epsilon_0 a_0^3)$. In these units the parameter $\gamma=U_{dd}/(\hbar^2/ma_0^2)$ plays the role of the dimensionless mass of the molecules.

Excitons. We start with the exciton Hamiltonian $H_{\rm exc}$ as defined in Eq. (15). In dimensionless units it is given by

$$H_{\rm exc}=\sum_i \tilde{E}_{eg}|e_i\rangle\langle e_i|+\frac{1}{2}\sum_{i\neq j}\frac{\hat{K}_{ij}}{|\mathbf{r}_i^0-\mathbf{r}_j^0|^3}, \tag{A1}$$

with $\tilde{E}_{eg}=\hbar\omega_{eg}/U_{dd}$ and $\hat{K}_{ij}$ defined in Eq. (13). In the limit of a low number of rotational excitations we can express $H_{\rm exc}$ in terms of the exciton operators $R_{\mathbf{k}}^\dagger=(1/\sqrt{N})\Sigma_i e^{i\mathbf{k}\mathbf{r}_i^0}|e_i\rangle\langle g_i|$ by making the substitutions

$$\hat{K}_{ij}\simeq\frac{1}{N}\sum_{\mathbf{k},\mathbf{k}'}R_{\mathbf{k}}^\dagger R_{\mathbf{k}'}[\epsilon(e^{-i(\mathbf{k}-\mathbf{k}')\mathbf{r}_i^0}+e^{-i(\mathbf{k}-\mathbf{k}')\mathbf{r}_j^0}) + \kappa(e^{+i\mathbf{k}'\mathbf{r}_i^0}e^{-i\mathbf{k}\mathbf{r}_j^0}+e^{+i\mathbf{k}'\mathbf{r}_j^0}e^{-i\mathbf{k}\mathbf{r}_i^0})], \tag{A2}$$

and $\Sigma_i|e_i\rangle\langle e_i|\simeq\Sigma_{\mathbf{k}}R_{\mathbf{k}}^\dagger R_{\mathbf{k}}$. Evaluating the resulting expressions we end up with a diagonal Hamiltonian of the form $H_{\rm exc}=\Sigma_{\mathbf{k}}E(\mathbf{k})R_{\mathbf{k}}^\dagger R_{\mathbf{k}}$, where the energy spectrum $E(\mathbf{k})=\tilde{E}_{eg}+\epsilon J(0)+\kappa J(\mathbf{k})$ is given in terms of the dimensionless function

$$J(\mathbf{k})=\sum_{i\neq 0}\frac{\cos(\mathbf{k}\mathbf{r}_i^0)}{|\mathbf{r}_i^0|^3}. \tag{A3}$$

For the 1D crystal with $r_i=i$ we can evaluate $J(k)$ and obtain

$$J(k)=2\sum_{j=1}^{\infty}\frac{\cos(kj)}{|j|^3}=\mathrm{Li}_3(e^{-ik})+\mathrm{Li}_3(e^{ik}), \tag{A4}$$

with $\mathrm{Li}_n(z)$ the polylogarithm function. In 2D the equilibrium positions $\mathbf{r}_i^0$ form a triangular lattice with basic lattice vectors

$a_1=(1,0)$ and $a_2=(1,\sqrt{3})/2$ and we evaluate the function $J(\mathbf{k})$ numerically (see Fig. 4). By replacing the summation in Eq. (A3) by an integral we obtain the linear behavior, $J(|\mathbf{k}|\to 0)-J(0)\sim|\mathbf{k}|$, for the long-wavelength limit. For a more detailed study of the spectrum of (rotational) excitons in 2D analytical tools developed in the field of 2D Wigner crystals [38] or 2D spin waves [39] can be applied to handle the slowly convergent sums in Eq. (A3). This analysis will be the subject of future work.

Phonons. In a next step we consider the Hamiltonian of longitudinal phonons, H_{phon}, which is given by

$$H_{\text{phon}}=\sum_i \frac{\mathbf{p}_i^2}{2\gamma}+\frac{3}{4}\sum_{i\neq j}\frac{5[(\mathbf{x}_i-\mathbf{x}_j)\cdot\mathbf{n}_{ij}^0]^2-[\mathbf{x}_i-\mathbf{x}_j]^2}{|\mathbf{r}_i^0-\mathbf{r}_j^0|^5}. \tag{A5}$$

As H_{phon} is quadratic in position and momentum operators we can rewrite it terms of phonon annihilation and creation operators, $H_{\text{phon}}=\Sigma_{\mathbf{q},\lambda}\hbar\omega_\lambda(\mathbf{q})a_\lambda^\dagger(\mathbf{q})a_\lambda(\mathbf{q})$. To find the phonon spectrum $\omega_\lambda(\mathbf{q})$ we change into the Heisenberg picture and make the ansatz

$$\mathbf{x}_i(t)=\frac{1}{\sqrt{N}}\sum_{\mathbf{q}}\sum_{\lambda=1}^{d}\sqrt{\frac{1}{2\gamma\omega_\lambda(\mathbf{q})}}\mathbf{e}_\lambda(\mathbf{q})[a_\lambda(\mathbf{q})e^{i[\mathbf{q}\cdot\mathbf{r}_i^0-\omega_\lambda(\mathbf{q})t]} + a_\lambda^\dagger(\mathbf{q})e^{-i[\mathbf{q}\cdot\mathbf{r}_i^0-\omega_\lambda(\mathbf{q})t]}], \tag{A6}$$

where in the 2D case the vectors $\mathbf{e}_\lambda(\mathbf{q})$ are the two orthonormal polarization vectors of the two phonon branches. This ansatz in combination with the Heisenberg equations $\ddot{\mathbf{x}}_i(t)=-[H_{\text{phon}},\mathbf{p}_i]/\gamma$ leads to the eigenvalue equation

$$-\omega_\lambda^2(\mathbf{q})\mathbf{e}_\lambda(\mathbf{q})=\mathcal{A}(\mathbf{q})\mathbf{e}_\lambda(\mathbf{q}). \tag{A7}$$

Here $\mathcal{A}(\mathbf{q})$ is a single valued function in 1D and a 2×2 matrix in 2D. For the 1D case we rewrite it as $\mathcal{A}(q)=f^2(q)/\gamma$ with

$$f^2(q)=48\sum_{j=1}^{\infty}\frac{\sin^2(qj/2)}{j^5}=12[2\zeta(5)-\text{Li}_5(e^{iq})-\text{Li}_5(e^{-iq})]. \tag{A8}$$

For the 2D crystal the matrix $\mathcal{A}(\mathbf{q})$ is defined as

$$\mathcal{A}(\mathbf{q})=\frac{3}{\gamma}\sum_{j\neq 0}\left[1-\frac{5}{|\mathbf{r}_j^0|^2}\begin{pmatrix}(x_j^0)^2 & x_j^0y_j^0\\ x_j^0y_j^0 & (y_j^0)^2\end{pmatrix}\right]\frac{(1-e^{i\mathbf{q}\cdot\mathbf{r}_j^0})}{|\mathbf{r}_j^0|^5}. \tag{A9}$$

By numerically solving the eigenvalue problem for the matrix $\mathcal{A}(\mathbf{q})$ for each value of $\mathbf{q}$ we obtain the two phonon branches $\omega_\lambda(\mathbf{q})$ and the corresponding polarization vectors $\mathbf{e}_\lambda$. In analogy to the 1D case we express the resulting phonon spectrum in terms of the two rescaled functions $f_\lambda(\mathbf{q})=\omega_\lambda(\mathbf{q})\sqrt{\gamma}$ (see Fig. 4).

Exciton-phonon interactions. Finally, we consider the first-order exciton-phonon interaction, H_{int}, given by

$$H_{\text{int}}=-\frac{3}{2}\sum_{i\neq j}\frac{\mathbf{r}_i^0-\mathbf{r}_j^0}{|\mathbf{r}_i^0-\mathbf{r}_j^0|^5}(\mathbf{x}_i-\mathbf{x}_j)\otimes\hat{K}_{ij}. \tag{A10}$$

Using Eqs. (A2) and (A6) we reexpress the interaction Hamiltonian in terms of exciton and phonon operators which leads us to the form of H_{int} given in Eq. (19) with a coupling matrix element

$$M_\lambda(\mathbf{q},\mathbf{k})=-\frac{3}{2}\sqrt{\frac{1}{2N\gamma\omega_\lambda(\mathbf{q})}}\sum_{j\neq 0}\frac{\mathbf{r}_j^0\cdot\mathbf{e}_\lambda(\mathbf{q})}{|\mathbf{r}_j^0|^5}(1-e^{i\mathbf{q}\cdot\mathbf{r}_j^0}) \times[\epsilon(1+e^{i\mathbf{q}\cdot\mathbf{r}_j^0})+\kappa(e^{-i(\mathbf{k}+\mathbf{q})\mathbf{r}_j^0}+e^{i\mathbf{k}\cdot\mathbf{r}_j^0})]. \tag{A11}$$

By introducing the function

$$g_\lambda(\mathbf{q})=\frac{3}{\sqrt{2}}\sum_{j\neq 0}\frac{\mathbf{r}_j^0\cdot\mathbf{e}_\lambda(\mathbf{q})}{|\mathbf{r}_j^0|^5}\sin(\mathbf{q}\mathbf{r}_j^0), \tag{A12}$$

we can bring $M_\lambda(\mathbf{q},\mathbf{k})$ into the form given in Eq. (25). For 1D we can evaluate the sum analytically,

$$g(q)=\frac{6}{\sqrt{2}}\sum_{j=1}^{\infty}\frac{\sin(qj)}{j^4}=\frac{3}{\sqrt{2}}[\text{Li}_4(e^{-iq})-\text{Li}_4(e^{+iq})]. \tag{A13}$$

In 2D the evaluation of the functions $g_\lambda(\mathbf{q})$ requires a numerical summation of the right-hand side of Eq. (A12).

APPENDIX B: EXCITON SPECTRUM OF A HARMONICALLY CONFINED MDC

In this appendix we derive approximate analytic expressions for the exciton spectrum in a harmonically confined dipolar crystal in 1D. All quantities in this appendix are expressed in units of the mean molecule separation at the center of the trap $a(0)=1/n(0)$ and the corresponding dipole-dipole energy U_{dd} (see Sec. V B 1).

We start with the exciton Hamiltonian H_{exc} given in Sec. V B in Eq. (45) and look at the eigenvalue equation $E(n)R_n^\dagger=[H_{\text{exc}},R_n^\dagger]$ for exciton operators $R_n^\dagger=\Sigma_i C_n(i)|e_i\rangle\langle g_i|$ with $n=1,\ldots,N$. In the limit of low number rotational excitons the resulting eigenvalue equation is of the form

$$[E(n)-\tilde{E}_{eg}]C_n(i)=\kappa\sum_{j\neq i}\frac{C_n(j)}{|x_i^0-x_j^0|^3}, \tag{B1}$$

with $\tilde{E}_{eg}=\hbar\omega_{eg}/U_{dd}$. For convenience we omit this constant energy offset in the following calculations. Our goal is to derive approximate analytic solutions of Eq. (B1) in the long- and short-wavelength limit.

Long-wavelength limit. For a large number of molecules N the density $n(x)$ varies slowly over the extension of the crystal and we make the approximation

$$\sum_{j\neq i}\frac{1}{|x_i^0-x_j^0|^3}\simeq 2\zeta(3)n^3(x_i^0), \tag{B2}$$

to convert Eq. (B1) into the form

$$[E(n) - 2\zeta(3)\kappa n^3(x_i^0)]C_n(i) = \kappa \sum_{j\neq i} \frac{C_n(j) - C_n(i)}{|x_j^0 - x_i^0|^3}. \quad \text{(B3)}$$

In the long-wavelength limit $C_n(x_i^0) \equiv C_n(i)$ can be approximated by a slowly varying continuous function $C_n(x)$ and

$$C_n(j) - C_n(i) \simeq C_n'(x_i^0)(x_j^0 - x_i^0) + C_n''(x_i^0)(x_j^0 - x_i^0)^2/2. \quad \text{(B4)}$$

Inserting this expansion into the right-hand side of Eq. (B3) we obtain two contributions. The first one proportional to the first derivative $C_n'(x)$ vanishes due to the summation over an equal number of terms with positive and negative sign. In contrast, the second contribution proportional to $C_n''(x)$ diverges as $\sim \ln(N)$. This divergence is a consequence of the long-range character of dipole-dipole interactions and means that Eq. (B3) is sensitive to the spatial extension of the wave function $C_n(x)$ and the expansion in Eq. (B4) will fail to predict accurate results. To handle this difficulty we proceed as follows. In a first step we approximate the divergent sum by

$$\sum_{j\neq i} \frac{1}{|x_i^0 - x_j^0|} = 2\Sigma_0 n(x_i^0), \quad \text{(B5)}$$

where in a zeroth-order approximation we set $\Sigma_0 = \ln(N/2)$. Under this approximation we find that (see below) wave functions $C_n(x)$ are harmonic oscillator eigenfunctions. In a second step we use the spatial dependence of these zeroth-order eigenfunctions for a more accurate reevaluation of the right-hand side of Eq. (B3).

Using the ansatz in Eq. (B5) we can convert the eigenvalue equation (B3) into the differential equation,

$$[E(n) - 2\zeta(3)\kappa n^3(x)]C_n(x) = \kappa\Sigma_0 n(x) C_n''(x). \quad \text{(B6)}$$

For the density profile $n(x)$ given in Eq. (53) and with a rescaled variable $y = 2x/L$ we obtain

$$C_n''(y) + b^2\left(\frac{\alpha_n - y^2}{(1-y^2)^{1/3}}\right)C_n(y) = 0, \quad \text{(B7)}$$

with $\alpha_n = 1 - E(n)/[2\zeta(3)\kappa]$ and $b^2 = \zeta(3)L^2/(2\Sigma_0)$. In a final approximation we expand Eq. (B7) to lowest order in y^2 and ϵ_n and end up with the differential equation

$$C_n''(y) + b^2(\alpha_n - y^2)C_n(y) = 0. \quad \text{(B8)}$$

Solutions of this equation are $C_n(x) \sim \Phi_n(x, \bar{\sigma})$ with $\bar{\sigma}^2 = L\sqrt{\Sigma_0/8\zeta(3)}$ and $\Phi_n(x, \bar{\sigma})$ the well-known harmonic oscillator functions

$$\Phi_n(x, \sigma) = H_{n-1}(x/\sigma)e^{-x^2/2\sigma^2}, \quad \text{(B9)}$$

with $H_n(x)$ Hermite polynomials. Using $L = \Lambda N$ the corresponding harmonic energy spectrum is

$$E(n) = \kappa\left(2\zeta(3) - \frac{\sqrt{32\zeta(3)\Sigma_0}}{\Lambda}\frac{(n-1/2)}{N}\right). \quad \text{(B10)}$$

At this point the energy spectrum $E(n)$ given in Eq. (B10) still depends on an inaccurately defined constant $\Sigma_0 \approx \ln(N/2)$ and its shape only poorly approximates the exact spectrum plotted in Fig. 7. As mentioned above this discrepancy is due to the fact that the cutoff radius for the sum given in Eq. (B5) is not determined by the size of the system, i.e., $r_c = N/2$, but rather by the shape of the wave function $C_n(x)$. To take into account this mode-dependent cutoff we use the following trick. First, for each mode function $C_n(x)$ we replace the constant Σ_0 in Eq. (B5) by $\Sigma(n)$, which has a different value for each mode n. Second, to derive an accurate expression for $\Sigma(n)$ we invert the expansion of $C_n(x_j^0)$ outlined in Eqs. (B3)–(B5) and express $\Sigma(n)$ in terms of the full wave function $C_n(x)$ as

$$\Sigma(n) = \frac{1}{n(x_i^0)C_n''(x_i^0)} \sum_{j\neq i} \frac{C_n(x_j^0) - C_n(x_i^0)}{|x_i^0 - x_j^0|^3}. \quad \text{(B11)}$$

To evaluate Eq. (B11) we focus on the region $x_i^0 \approx 0$ and neglect small variations of the density. For the mode functions $C_n(x)$ we insert the harmonic oscillator functions, $C_n(x) \sim \Phi_n(x, \bar{\sigma})$, derived above. Around the center of the trap we can further approximate these wave functions by $C_n(x) \sim \cos(k_n x)$ [or $C_n(x) \sim \sin(k_n x)$ for odd n] with a wave vector $k_n^2 = (2n-1)/\bar{\sigma}^2$. For even modes this approximation results in

$$\Sigma(n) \simeq \frac{1}{k_n^2}\left(2\zeta(3) - \sum_{j\neq 0} \frac{\cos(k_n j)}{|j|^3}\right), \quad \text{(B12)}$$

which can now be evaluated in a closed form in terms of polylogarithm functions [see Appendix A, Eq. (A4)]. Expanding the result to lowest order in k_n we finally obtain

$$\Sigma(n) \simeq \frac{1}{2}\left[3 + \ln\left(\frac{\bar{\sigma}^2}{2n-1}\right)\right]. \quad \text{(B13)}$$

By replacing Σ_0 with $\Sigma(n)$ in Eq. (B10) we end up with the improved exciton spectrum

$$E(n) = \kappa\left[2\zeta(3) - A\sqrt{B_N + \ln\left(\frac{N}{n-1/2}\right)}\frac{(n-1/2)}{N}\right], \quad \text{(B14)}$$

with $B_N = 3 + \ln[\Lambda\sqrt{\ln(N/2)/32\zeta(3)}]$ and $A = 4\sqrt{\zeta(3)}/\Lambda$. The corresponding improved mode functions are given by $C_n(x) \sim \Phi_n(x, \sigma_n)$ with a n-dependent width

$$\sigma_n^2 = N\frac{\Lambda}{4\sqrt{\zeta(3)}}\left[B_N + \ln\left(\frac{N}{n-1/2}\right)\right]^{1/2}. \quad \text{(B15)}$$

Although our derivation was based on several rather crude approximations we find in comparison with numerics that our analytic solutions for $E(n)$ and $C_n(x)$ provide an accurate description of the long-wavelength behavior of the exciton spectrum and the shape of the eigenfunctions. Due to the similarity of the underlying equations this approach should also be applicable to improve the linear phonon spectrum obtained in Ref. [33] for a harmonically confined ion crystal.

Short-wavelength limit. For the short-wavelength limit of the exciton spectrum we make the ansatz $C_n(x_i^0) \equiv C_n(i) = (-1)^i \tilde{C}_n(x_i^0)$ such that $\tilde{C}_n(x)$ represents a slowly varying envelope function for the rapidly oscillating mode function

$C_n(x)$. Inserting this ansatz into the eigenvalue equation (B1) we can proceed in the derivation of $\tilde{C}_n(x)$ as explained above for the long-wavelength limit. However, in the short-wavelength limit the fast oscillating eigenmodes cancel the effect of long-range interactions and in contrast to the divergent sum in Eq. (B5) the corresponding term in the short-wavelength limit has a well-defined value,

$$\frac{1}{2}\sum_{j\neq i}\frac{(-1)^{i-j}}{|x_i^0-x_j^0|}\simeq -\ln(2)n(x_i^0). \tag{B16}$$

Therefore, the resulting spectrum in the short-wavelength limit is purely harmonic and has the form

$$E(n)=\kappa\left(-\frac{3\zeta(3)}{2}+\frac{\sqrt{24\zeta(3)\ln(2)}}{\Lambda}\frac{(\bar{n}-1/2)}{N}\right), \tag{B17}$$

with $\bar{n}=N-n+1$. The envelop functions $\tilde{C}_n(x)\sim\Phi_{\bar{n}}(x,\sigma)$ are harmonic oscillator eigenfunctions with a width

$$\sigma^2=N\Lambda\sqrt{\ln(2)/6\zeta(3)}. \tag{B18}$$

APPENDIX C: PHONON SPECTRUM OF A HARMONICALLY CONFINED MDC

In this appendix we derive approximate analytic expressions for the spectrum of longitudinal and transverse phonons in a harmonically confined MDC. Our calculations are based on a similar approach used in Ref. [33] for the phonon spectrum of a 1D ion crystal. However, in contrast to the ion crystal or the exciton spectrum derived in Appendix B, the long-range character of dipole-dipole interactions has no severe effect on the phonon spectrum of a dipolar crystal which simplifies calculations. Here we outline only the derivation of the spectrum of longitudinal phonons. The spectrum of transverse phonons can be derived along the same lines and we give the results at the end of this appendix. Note that throughout this appendix we express results in units of $a(0)=1/n(0)$ and U_{dd} as defined in Sec. V B 1.

To derive the eigenspectrum $\omega(m)$ with $m=1,\ldots,N$ of the Hamiltonian $H_{\mathrm{phon}}^{\parallel}$ given in Eq. (46) we change into the Heisenberg picture where position operators $x_i(t)$ obey the equation of motion,

$$\ddot{x}_i(t)=-\tilde{\nu}^2x_i(t)-\frac{12}{\gamma}\sum_{j\neq i}\frac{x_i(t)-x_j(t)}{|x_i^0-x_j^0|^5}, \tag{C1}$$

with $\tilde{\nu}=\hbar\nu/U_{dd}$ the normalized trapping frequency. Using the normal mode decomposition given in Eq. (50), Eq. (C1) translates into the eigenvalue equation,

$$\gamma[\tilde{\nu}^2-\omega^2(m)]c_m(i)=-12\sum_{j\neq i}\frac{c_m(i)-c_m(j)}{|x_i^0-x_j^0|^5}, \tag{C2}$$

for the normal modes $c_m(i)$. In the long-wavelength limit we can replace the discrete set of coefficients $c_m(x_i^0)\equiv c_m(i)$ by a continuous function $c_m(x)$ and make the approximation

$$c_m(j)\simeq c_m(i)+c'(x_i^0)(x_j^0-x_i^0)+c''(x_i^0)(x_j^0-x_i^0)^2/2. \tag{C3}$$

As the mode functions of long-wavelength phonons extend over the whole length of the crystal we include variations of the density $n(x)$ given in Eq. (53), i.e.,

$$x_j^0-x_i^0\simeq\frac{(j-i)}{n(x_i^0)}-\frac{(j-i)^2}{2}\frac{n'(x_i^0)}{n^3(x_i^0)}. \tag{C4}$$

Keeping terms up to second order in the derivatives $c_m'(x)$ and $n'(x)$, Eq. (C2) transforms into the differential equation

$$n^3(y)c_m''(y)+4n^2(y)n'(y)c_m'(y)-\alpha_m c_m(y)=0, \tag{C5}$$

with $y=2x/L$ and $\alpha_m=2[1-\omega^2(m)/\tilde{\nu}^2]/3$. Here we made use of the identity $\gamma\tilde{\nu}^2L^2=32\zeta(3)$ [see Sec. V B 1, Eq. (56)]. For the density $n(y)=\sqrt[3]{1-y^2}$ we find $n^2(y)n'(y)\simeq-2/3y$ and the differential equation (C5) can be solved by the ansatz $c_m(y)=\Sigma_k a_k y^k$. The coefficients obey the recursion rule

$$a_{k+2}=a_k[k(k-1)+8k/3+\alpha_m]/(k+1)(k+2).$$

The quantization condition for mode m, $a_{k+2}=0$, $\forall\ k>m-1$, follows from the normalizability of the resulting polynomials and translates into the spectrum

$$\omega(m)=\tilde{\nu}\sqrt{1+(3m^2-m-2)/2}. \tag{C6}$$

The corresponding mode functions $c_m(x)$ are polynomials extended over the whole length of the crystal.

In the short-wavelength limit we make the ansatz $c_m(i)=(-1)^i\tilde{c}_m(x_i^0)$ and repeat the calculations from above for the slowly varying envelope function $\tilde{c}_m(x)$. For $y=2x/L$ we obtain

$$\tilde{c}_m''(y)+\frac{4n'(y)}{3n(y)}\tilde{c}_m'(y)+\frac{[\beta N^2n^5(y)+\alpha_m]}{n^3(y)}\tilde{c}_m(y)=0, \tag{C7}$$

with $\beta=31\zeta(5)\Lambda^2/24\zeta(3)$ and $\alpha_m=8[1-\omega^2(m)/\tilde{\nu}^2]/9$. We can simplify Eq. (C7) by neglecting the term proportional to $n'(y)$ and by expanding the remaining equation up to second order in y. This approximation is valid, since we will find below, that the mode functions of short-wavelength phonons are located at the center of the chain. We end up with

$$\tilde{c}_m''(y)+[N^2\beta+\alpha_m-(2N^2\beta/3-\alpha_m)y^2]\tilde{c}_m(y)=0. \tag{C8}$$

Solutions of this equation are of the form

$$\tilde{c}_m(x)\sim H_{\bar{m}}(x/\sigma)e^{-x^2/2\sigma^2}, \tag{C9}$$

with $\bar{m}=N-m$ and $\sigma^2=N\lambda^2\sqrt{3/(80\beta)}$. The corresponding spectrum is given by

$$\omega(m)\simeq\omega_D\left(1-\sqrt{\frac{5}{3\beta}}\frac{(\bar{m}+1/2)}{N}\right), \tag{C10}$$

with a Debye frequency $\omega_D=\tilde{\nu}N\sqrt{9\beta/8}$.

Transverse phonons. Along the same lines as shown for the longitudinal phonons we calculate analytic expressions for the spectrum of transverse phonons determined by the

Hamiltonian $H^{\perp}_{\mathrm{phon}}$ given in Eq. (47). In the long-wavelength limit the resulting spectrum is

$$\omega^{\perp}_{y,z}(m) \simeq \sqrt{\tilde{\nu}^2_{\perp} - \alpha_{y,z}\frac{4\zeta(3)}{\gamma}\frac{(3m^2-m-2)}{N^2}}, \quad \text{(C11)}$$

with $\alpha_y=1$, $\alpha_z=3$, and $\tilde{\nu}_{\perp}=\hbar\nu_{\perp}/U_{dd}$. For the short-wavelength limit we obtain a spectrum of the form

$$\omega^{\perp}_{y,z}(m) \simeq \sqrt{\tilde{\nu}^2_{\perp} - A\frac{\alpha_{y,z}}{\gamma}\left(1 - B\frac{(\bar{m}+1/2)}{N}\right)} \quad \text{(C12)}$$

with numerical constants $A=93\zeta(5)/8\simeq 12.05$ and $B=\sqrt{5\zeta(3)32/31\zeta(5)}\simeq 2.055$.

APPENDIX D: LINDEMANN PARAMETER

In this appendix we calculate the local Lindemann parameter $\Gamma_L(x,T)$ as defined in Eq. (63) both for the homogeneous and the inhomogeneous crystal. Note that in the following we express all quantities in units of a_0 and U_{dd}. Using the normal mode decomposition of operators x_i given in Eq. (A6) for the homogeneous system and in Eq. (50) for the inhomogeneous case we obtain

$$\Gamma^2_L(x^0_i,T) = \sum_k \frac{n(x^0_i)}{2\gamma\omega(k)}|c_k(i+1)-c_k(i)|^2[2N(\omega(k))+1], \quad \text{(D1)}$$

with $N(\omega(k))$ the thermal occupation number of mode k. For a homogenous system k is the quasimomentum, $c_k(i)$ are plane waves, and $\omega(k)=f(k)/\sqrt{\gamma}$. In the homogeneous system we replace k by the index $m=1,\ldots,N$ and the normal modes $c_m(i)$ with the corresponding spectrum $\omega(m)$ are discussed in Sec. V B and Appendix C. For simplicity we adopt the sound wave approximation $\omega(m)\simeq[\alpha_D/\sqrt{\gamma}]m/N$ with $\alpha_D\approx 6.95$. The Lindemann parameter then has the general form

$$\Gamma_L(x,T) = \frac{1}{\gamma^{1/4}}F(\xi=2x/L,\tau=\sqrt{\gamma}T). \quad \text{(D2)}$$

For the homogeneous crystal $F(\xi,\tau)=F_h(\tau)$ with

$$F^2_h(\tau) = \frac{2}{\pi}\int_0^{\pi}\frac{dk}{f(k)}\sin^2(k/2)\left(\frac{2}{e^{f(k)/\tau}-1}+1\right). \quad \text{(D3)}$$

In the two limits of interest the numerical values of this function are $F_h(\tau\to 0)\simeq 0.424$ and $F_h(\tau\gg 1)\simeq 0.278\sqrt{\tau}$. In the inhomogeneous case we obtain

$$F^2(\xi,\tau) = \frac{2}{N\alpha_D\Lambda^2}\sum_m \frac{[c'_m(\xi)]^2}{n(\xi)m}\left(\frac{2}{e^{\alpha_D m/(\tau N)}-1}+1\right). \quad \text{(D4)}$$

Numerical values of this function are plotted in Fig. 9.

[1] A. Andre, D. DeMille, J. M. Doyle, M. D. Lukin, S. E. Maxwell, P. Rabl, R. Schoelkopf, and P. Zoller, Nat. Phys. **2**, 636 (2006).
[2] P. Rabl, D. DeMille, J. M. Doyle, M. D. Lukin, R. J. Schoelkopf, and P. Zoller, Phys. Rev. Lett. **97**, 033003 (2006).
[3] Yu. Makhlin, A. Shnirman, and G. Schön, Rev. Mod. Phys. **73**, 357 (2001).
[4] D. Vion, A. Aassime, A. Cottet, P. Joyez, H. Pothier, C. Urbina, D. Esteve, and M. H. Devoret, Science **296**, 886 (2002).
[5] T. Yamamoto, Yu. A. Pashkin, O. Astafiev, Y. Nakamura, and J. S. Tsai, Nature (London) **425**, 941 (2003).
[6] A. Wallraff, D. I. Schuster, A. Blais, L. Frunzio, R. S. Huang, J. Majer, S. Kumar, S. M. Girvin, and R. J. Schoelkopf, Nature (London) **431**, 162 (2004).
[7] I. Chiorescu, P. Bertet, K. Semba, Y. Nakamura, C. J. P. M. Harmans, and J. E. Mooij, Nature (London) **431**, 159 (2004).
[8] D. Loss and D. P. DiVincenzo, Phys. Rev. A **57**, 120 (1998).
[9] J. R. Petta, A. C. Johnson, J. M. Taylor, E. A. Laird, A. Yacoby, M. D. Lukin, C. M. Marcus, M. P. Hanson, and A. C. Gossard, Science **309**, 2180 (2005).
[10] F. H. L. Koppens, C. Buizert, K. J. Tielrooij, I. T. Vink, K. C. Nowack, T. Meunier, L. P. Kouwenhoven, and L. M. K. Vandersypen, Nature (London) **442**, 766 (2006).
[11] G. Burkard and A. Imamoglu, Phys. Rev. B **74**, 041307(R) (2006).
[12] For alternative approaches to hybrid quantum computing see A. S. Sorensen, C. H. van der Wal, L. I. Childress, and M. D. Lukin, Phys. Rev. Lett. **92**, 063601 (2004); L. Tian, P. Rabl, R. Blatt, and P. Zoller, *ibid.* **92**, 247902 (2004).
[13] D. H. E. Dubin and T. M. O'Neil, Rev. Mod. Phys. **71**, 87 (1999).
[14] W. J. Wallace and R. H. Silsbee, Rev. Sci. Instrum. **62**, 1754 (1991).
[15] L. Frunzio, A. Wallraff, D. Schuster, J. Majer, and R. Schoelkopf, IEEE Trans. Appl. Supercond. **15**, 860 (2005).
[16] A. A. Houck *et al.*, arXiv:cond-mat/0702648.
[17] H. P. Büchler, E. Demler, M. Lukin, A. Micheli, N. Prokof'ev, G. Pupillo, and P. Zoller, Phys. Rev. Lett. **98**, 060404 (2007).
[18] A. Micheli, G. Pupillo, H. P. Büchler, and P. Zoller, arXiv:quant-ph/0703031.
[19] A. S. Arkhipov, G. E. Astrakharchik, A. V. Belikov, and Yu. E. Lozovik, JETP Lett. **82**, 39 (2005).
[20] R. Citro, E. Orignac, S. De Palo, and M. L. Chiofalo, Phys. Rev. A **75**, 051602(R) (2007).
[21] G. E. Astrakharchik, J. Boronat, I. L. Kurbakov, and Yu. E. Lozovik, Phys. Rev. Lett. **98**, 060405 (2007).
[22] J. M. Brown and A. Carrington, *Rotational Spectroscopy of Diatomic Molecules* (Cambridge University Press, Cambridge, 2003); G. Herzberg, *Spectra of Diatomic Molecules* (Van Nostrand, Princeton, NJ, 1950).

[23] J. Knoester and V. M. Agranovich, "Electronic excitations in organic based nanostructures," in *Thin Films and Nanostructures*, edited by V. M. Agranovich and G. F. Bassani (Elsevier, San Diego, 2003), Vol. 31.
[24] See, for example, G. D. Mahan, *Many-Particle Physics* (Kluwer Academic/Plenum, New York, 2000).
[25] R. K. Kalia and P. Vashishta, J. Phys. C **14**, L643 (1981).
[26] For a review on experimental progress in the field of cold molecules see J. Doyle, B. Friedrich, R. V. Krems, and F. Masnou-Seeuws, Eur. Phys. J. D **31**, 149 (2004), and references cited.
[27] R. V. Krems, A. Dalgarno, N. Balakrishnan, and G. C. Groenenboom, Phys. Rev. A **67**, 060703(R) (2003).
[28] A. Micheli, G. K. Brennen, and P. Zoller, Nat. Phys. **2**, 341 (2006).
[29] D. M. Harber, H. J. Lewandowski, J. M. McGuirk, and E. A. Cornell, Phys. Rev. A **66**, 053616 (2002).
[30] P. Treutlein, P. Hommelhoff, T. Steinmetz, T. W. Hänsch, and J. Reichel, Phys. Rev. Lett. **92**, 203005 (2004).
[31] C. Langer *et al.*, Phys. Rev. Lett. **95**, 060502 (2005).
[32] H. Häffner *et al.*, Appl. Phys. B: Lasers Opt. **81**, 151 (2005).
[33] G. Morigi and S. Fishman, Phys. Rev. E **70**, 066141 (2004).
[34] D. H. E. Dubin, Phys. Rev. Lett. **71**, 2753 (1993).
[35] J. P. Schiffer, Phys. Rev. Lett. **70**, 818 (1993).
[36] D. G. Enzer *et al.*, Phys. Rev. Lett. **85**, 2466 (2000).
[37] See, for example, E. Knill, Nature (London) **434**, 39 (2005), and references therein.
[38] L. Bonsall and A. A. Maradudin, Phys. Rev. B **15**, 1959 (1977).
[39] H. Benson and D. L. Mills, Phys. Rev. **178**, 839 (1969).